THERMAL BUCKLING OF LAMINATED PLATES WITH VARIABLE FIBER VOLUME FRACTION

A THESIS SUBMITTED TO
THE GRADUATE SCHOOL OF NATURAL AND APPLIED SCIENCES
OF
MIDDLE EAST TECHNICAL UNIVERSITY

BY

EMRULLAH MERCAN

IN PARTIAL FULFILLMENT OF THE REQUIREMENTS
FOR
THE DEGREE OF MASTER OF SCIENCE
IN
MECHANICAL ENGINEERING

JANUARY 2023

Approval of the thesis:

THERMAL BUCKLING OF LAMINATED PLATES WITH VARIABLE FIBER VOLUME FRACTION

submitted by **EMRULLAH MERCAN** in partial fulfillment of the requirements for the degree of **Master of Science** i**n Mechanical Engineering, Middle East Technical University** by,

Prof. Dr. Halil Kalıpçılar
Dean, Graduate School of **Natural and Applied Sciences** _____

Prof. Dr. M.A. Sahir Arıkan
Head of the Department, **Mechanical Engineering** _____

Prof. Dr. Serkan Dağ
Supervisor, **Mechanical Engineering Dept, METU** _____

Examining Committee Members:

Assoc. Prof. Dr. Merve Erdal
Mechanical Engineering, METU _____

Prof. Dr. Serkan Dağ
Mechanical Engineering, METU _____

Assoc. Prof. Dr. Ulaş Yaman
Mechanical Engineering, METU _____

Assist. Prof. Dr. Gökhan Özgen
Mechanical Engineering, METU _____

Assoc. Prof. Dr. Tunç Apatay
Mechanical Engineering, Gazi Uni. _____

Date: 27.01.2023

I hereby declare that all information in this document has been obtained and presented in accordance with academic rules and ethical conduct. I also declare that, as required by these rules and conduct, I have fully cited and referenced all material and results that are not original to this work.

Name Last name : Emrullah Mercan

Signature :

ABSTRACT

THERMAL BUCKLING OF LAMINATED PLATES WITH VARIABLE FIBER VOLUME FRACTION

Mercan, Emrullah
Master of Science, Mechanical Engineering
Supervisor : Prof. Dr. Serkan Dağ

January 2023, 87 pages

This study investigates the stability of the graded fiber reinforcement composite plate under temperature-induced loads. The materials that make up the graded fiber reinforcement composite plate are fiber and matrix with different mechanical properties. Graduation is achieved by varying the volume fractions of the components across the thickness. The symmetric and unsymmetric ply sequences in the modeled composite plate are examined separately. Governing equations of motion and boundary conditions are obtained using Hamilton's principle. The displacement equations are obtained using Kirchhoff deformation theory. The system of equations written for the modeled case is solved numerically using the differential quadrature method. In order to validate the examined model, the studies in the literature and the models prepared in Abaqus are compared. Then, critical buckling temperature values for graded fiber reinforcement composite plate exposed to uniform temperature increase are found using MATLAB. According to the results obtained, the graduation in the thickness direction affects the thermal strength of the structure. The expected critical buckling temperature value increases as the plate is graded throughout the thickness.

Keywords: Graded fiber reinforcement composite plate, Kirchhoff plate theory, Differential quadrature method, Critical buckling temperature, Ply orientation

ÖZ

DEĞİŞKEN ELYAF HACMİNE SAHİP LAMİNE LEVHALARIN TERMAL BURKULMASI

Mercan, Emrullah
Yüksek Lisans, Makina Mühendisliği
Tez Yöneticisi: Prof. Dr. Serkan Dağ

Ocak 2023, 87 sayfa

Bu çalışma, kademeli fiber takviyeli kompozit levhanın sıcaklığa bağlı yükler altındaki stabilitesini araştırmaktadır. Kademeli elyaf takviyeli kompozit levhayı oluşturan malzemeler, farklı mekanik özelliklere sahip elyaf ve matristir. Derecelendirme, kalınlık boyunca bileşenlerin hacim fraksiyonlarını değiştirerek elde edilir. Modellenen kompozit plakadaki simetrik ve simetrik olmayan kat dizileri ayrı ayrı incelenmiştir. Hareket denklemleri ve sınır koşulları Hamilton prensibi kullanılarak elde edilir. Yer değiştirme denklemleri, Kirchhoff deformasyon teorisi kullanılarak elde edilir. Modellenen durum için yazılan denklem sistemi, diferansiyel kareleme yöntemi kullanılarak sayısal olarak çözülür. İncelenen modeli doğrulamak için literatürdeki çalışmalar ile Abaqus'te hazırlanan modeller karşılaştırılmıştır. Daha sonra MATLAB kullanılarak üniform sıcaklık artışına maruz kalan kademeli fiber takviyeli kompozit levha için kritik burkulma sıcaklık değerleri bulunmuştur. Elde edilen sonuçlara göre kalınlık yönündeki derecelenme yapının ısıl dayanımını etkilemektedir. Beklenen kritik burkulma sıcaklığı değeri, levha kalınlık boyunca derecelendirildikçe artar.

Anahtar Kelimeler: Kademeli elyaf takviyeli kompozit levha, Kirchhoff levha teorisi, Diferansiyel kareleme yöntemi, Kritik burkulma sıcaklığı, Kat oryantasyonu

To My Family

ACKNOWLEDGMENTS

First of all, I am deeply grateful to my thesis supervisor Prof. Dr. Serkan Dağ, for accepting to work with me, guiding me within the scope of my research, adding depth to my studies, and always giving his support in this regard.

I would like to thank the Dr. Reza Aghazadeh for supporting me in my research, giving me ideas for my studies, and helping me be motivated about the problems I encountered.

I would also like to thank the examining committee members for their contributions and comments.

I would like to thank my friends and my work team, whose support and love I have felt closely throughout my academic life.

The most significant contributor to my work is undoubtedly my family. I would like to thank my family for always caring about me, trusting and supporting me regardless of the success or failures I have encountered.

TABLE OF CONTENTS

LIST OF TABLES

TABLES

LIST OF FIGURES

FIGURES

LIST OF ABBREVIATIONS

SSSS	All edges simply supported
CCCC	All edges clamped
DQM	Differential quadrature method
FRC	Fiber – reinforced composite
FEA	Finite element analysis

LIST OF SYMBOLS

$\boldsymbol{a}$	Length of plate
$\boldsymbol{b}$	Width of plate
$\boldsymbol{h}$	Thickness of plate
$\boldsymbol{u, v, w}$	Displacement of plate in x, y, z directions
$\boldsymbol{u_0, v_0, w_0}$	Displacement of mid-plane in x, y, z directions
$\boldsymbol{\varepsilon_{ij}}$	Strain tensor
$\boldsymbol{\sigma_{ij}}$	Stress tensor
$\boldsymbol{Q_{ij}}$	Plane stress-reduced stiffness
$\boldsymbol{\alpha_{xx}, \alpha_{yy}, \alpha_{xy}}$	Thermal expansion coefficients
$\boldsymbol{\bar{Q}_{ij}}$	Transformed plane stress-reduced stiffness
$\boldsymbol{\delta U}$	Strain energy variation
$\boldsymbol{\delta\varepsilon_{ij}}$	Virtual strain
$\boldsymbol{N(w)}$	Prebuckling thermal force resultants
$\boldsymbol{N_{ij}}$	Resultant forces
$\boldsymbol{\bar{N}_{ij}^{T}}$	Force resulting from thermal effect
$\boldsymbol{M_{ij}}$	Resultant moments
$\boldsymbol{\Delta T}$	Temperature difference
$\boldsymbol{A_{ij}}$	Extensional stiffness
$\boldsymbol{D_{ij}}$	Bending stiffness

$\boldsymbol{B_{ij}}$	Bending extensional coupling stiffness
$\boldsymbol{A_x, A_y, A_{xy}}$	Thermal stiffness
$\boldsymbol{A_{ij}^{(n)}}$	Weighting coefficients of n^{th} derivative
$\boldsymbol{x_i}$	Set of discrete point in x direction
N	Number of sampling points
$\boldsymbol{M^{(1)}}$	Lagrangian interpolation shape function
K	Stiffness matrix
P	Critical buckling load
W	Buckling mode shape
$\boldsymbol{V_f}$	Fiber volume fraction
$\boldsymbol{E^f}$	Fiber young modulus
$\boldsymbol{G^f}$	Fiber shear modulus
$\boldsymbol{v^f}$	Fiber poisson's ratio
$\boldsymbol{E^m}$	Matrix young modulus
$\boldsymbol{G^m}$	Matrix shear modulus
$\boldsymbol{v^m}$	Matrix poisson's ratio
$\boldsymbol{\alpha^f}$	Fiber thermal expansion coefficient
$\boldsymbol{\alpha^m}$	Matrix thermal expansion coefficient
$\boldsymbol{E_{11}}$	Longitudinal modulus
$\boldsymbol{E_{22}}$	Transverse modulus
$\boldsymbol{G_{12}}$	In-plane shear modulus

$\boldsymbol{v_{12}}$	Poisson ratio
$\boldsymbol{\alpha_1}$	Longitudinal thermal expansion coefficient
$\boldsymbol{\alpha_2}$	Transverse thermal expansion coefficient

CHAPTER 1

INTRODUCTION

1.1 Introduction

Composite materials have recently entered our lives, and their use is becoming more common. These materials are superior in many ways and are highly preferred. Composite materials are primarily used in structural elements design, as they provide features such as a high stiffness-to-weight ratio. There are many types of composite materials, one of which is fiber-reinforced composite materials. Fiber reinforcement composite materials are used to obtain more suitable designs for structures with high stress and free vibration. The multitude of advantageous aspects of fiber-structured materials has led to their evaluation in another way. These materials can be graded in different directions by adding a new concept to fiber-reinforced composite materials. This gradation is achieved by changing the fiber volume fraction in the thickness direction. As a result, composite materials with mechanical properties from strong to weak can be derived. Thanks to this grading, more optimum designs can be obtained.

Similar situations are observed in the industry in this regard. Electronic equipment in aircraft is exposed to high thermal loads. While some surfaces of these electronic packages are exposed to higher temperature, some surfaces are exposed to lower temperature. Due to the surface temperature difference, a force occurs on the structure. This force causes buckling in the structure. For this reason, the thermal resistance of the surface exposed to high temperatures should be higher, while the thermal resistance of the surface exposed to lower temperatures should be less. Based on this, graded fiber-reinforced composite materials are produced.

Fiber-reinforced composite materials consist of fibers and matrices. These materials are obtained by combining fibers and matrices in certain proportions. In order to get the desired properties, fiber and matrix amounts and types are selected accordingly, and appropriate material is obtained. Graded fiber-reinforced composite materials, on the other hand, consist of fibers and matrices with different volume fractions in each layer, and this grading is applied throughout the thickness. In this way, the material shows different mechanical properties throughout the thickness. In addition, the laying angle of each layer can be different, and accordingly, symmetrical and unsymmetric graded composite materials are obtained. The mechanical behavior of these two different composite materials also differs. Within the scope of the thesis, there will be studies on the behavior of symmetrical and unsymmetric graded fiber-reinforced composite materials. Thermal buckling of laminated plates with variable fiber volume fraction for the symmetric and unsymmetric laminated plates will be investigated. Buckling is an important subject and affects the structure's load-carrying capacity. A configuration of the buckled plate is shown in Figure 1.1. When a plate is exposed to buckling, the plate's buckled point becomes concave shaped, named bending mode. After buckling, the applied load is redistributed with respect to changes in stiffness values of the remaining surface and bended surface. The stiffness of the remaining part of the structure is quite higher than the bended surface. Therefore, most of the applied forces are carried by the remaining part, and a little part of the applied forces are carried by the bended surface. Deforming of buckled shape is easier than a flat shape because of the height of concavity, which causes extra bending forces.

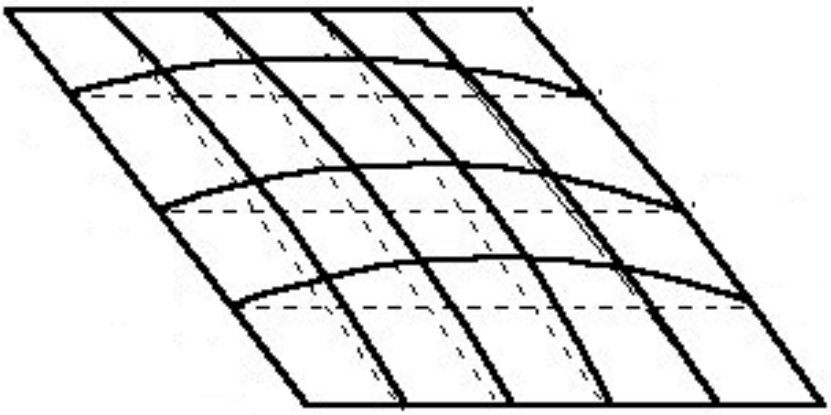

Figure 1.1. Buckle state of plate

1.2 Literature Survey

Many researchers have studied fiber-reinforced composite materials. Shen and Yang [1] investigated the linear and nonlinear free flexural vibration behavior of cylindrical shell made of the fiber-reinforced composite under hygrothermal conditions. In this study, equations of motion were obtained using higher-order shear deformation shell theory and von Karman type of kinematic nonlinearity. According to the results obtained, temperature/moisture variation has a moderate effect on the natural frequencies of the FRC cylindrical shell. In a paper, large amplitude vibration, nonlinear bending, and thermal post-buckling of fiber-reinforced composite beams resting on an elastic foundation in hygrothermal environments are studied [2]. In another research, Shen, and Zhang [3] performed a nonlinear analysis for the fiber-reinforced composite laminated plate. Uniformly distributed and functionally graded reinforcement laminated plates were examined separately. In a study by Yas and Aragh [4], free vibration characteristics of continuous grading fiber-reinforced plates resting on an elastic foundation are studied. The results of the research were obtained by using three-dimensional, linear, and small strain elasticity theory. Nejati et al. [5] developed a model based on the three-dimensional theory of elasticity to study the free vibration of reinforced functionally graded composite

plates with steady-state thermal conditions. Yas and Aragh [6] studied the thermoelastic behavior of functionally graded fiber-reinforced cylindrical panel in a steady state using the differential quadrature method. They concluded that functionally graded fiber-reinforced composite structures are better than discretely laminated composite panels. In research conducted by Fu et al. [7], the effect of non-uniform fiber distribution on the stress distribution of the structure was studied. It was observed that while in-plane stress was affected by fiber distribution, transverse stress was not affected much. Based on Reddy's higher-order shear deformation theory, Tang et al. [8] investigated the hygrothermal effect on geometrically nonlinear analysis of CFRP laminates. Using Von Karman large deflection assumptions and quasi-steady state supersonic aerodynamic theory, Kuo [9] examined the effect of variable fiber spacing on thermal post-buckling, vibration, and flutter. The structure exposed to aerodynamic and thermal stress shows different behaviors according to the fiber distribution. It has been observed that the redistribution of fiber increases the natural frequencies and flutter boundary.

The study mentioned above examined the benefits and usage areas of fiber-reinforced composite material. As understood from the researchers' studies, these materials provide many advantages in design. The most common application of composite materials is the areas where buckling occurs. The deterioration of the stability of the structure is called buckling, and it is considered a failure in engineering. Depending on the material of the examined structure, the buckling status may change. From this point of view, composite materials are suitable for use in places where buckling is expected since they show the desired resistance. There are many studies on the behavior of composite materials in the buckling state.

Some of these studies are described as follows. Leissa [10] has done a study on the buckling behavior of symmetrically laminated composite plates using orthotropic and anisotropic plate buckling theory. In articles by Altunsaray et al. [11] the buckling behavior of symmetrically laminated rectangular thin plates under biaxial compression was investigated. Using the Rayleigh-Ritz method, the researchers calculated the critical buckling load of simply supported cross-ply and angle ply

plates according to classical lamination theory. Based on classical lamination plate theory, Raju et al. [12] studied the buckling resistance of variable angle tow plate under different boundary conditions. In this study, Airy's stress function was used as an innovation, and prebuckling analysis was performed in a shorter time. In another research, Fares and Zenkour [13] used various theories of the homogeneous laminated plate to examine the buckling and free vibration behavior of non-homogeneous rectangular composite plates. The study concludes that the classical lamination plate theory is insufficient to predict the structural behavior of non-homogeneous laminates. Sheehari et al. [14] also conducted a study on the analysis of buckling and post-buckling of laminated composite plates under hygrothermal load, using inverse hyperbolic shear deformation theory. In theory used, the non-linear stress distribution is obtained by providing zero transverse stress condition on the top and bottom surface. Kazemi [15] did a similar study. In the study, buckling and post-buckling analyses were performed for composite laminate using modified shear deformation theory. Another study was done by Han et al [16]. In the article published by the researchers, buckling analyses were performed for the variable angle laminated plate exposed to compression load, and the behavior of the plate was investigated. The analysis results show that the maximum in-plane stress of variable angle laminates decreases, and the buckling load increases considerably. In research conducted by Kumar [17] using higher-order shear deformation plate theory, the effect of moisture and temperature on the buckling behavior of the laminated composite plate was investigated. Buckling analysis was performed at different boundary conditions for restrained laminated rectangular plates resting on an elastic Pasternak foundation. Using the genetic algorithm method, the ideal stacking sequence to increase the buckling strength of the structure was determined [18]. In the study, Grah and Weaver [19] studied the buckling behavior of laminate with one-dimensional fiber variation and laminate with symmetric stacking sequences, taking the transverse shear effect into account in their calculations. According to the result of the research, the buckling behavior of variable angle tow and variable thickness laminates can be better expressed by shell-like behavior rather than plate-like. In a

study by Qunis et al. [20], the issue of buckling was also discussed. The thermal buckling situation for a composite laminated plate with uniform temperature distribution has been examined. It is a study using the finite element method, and validation has been done with similar studies in the literature. Shiau [21] has also done buckling and vibration studies for composite laminated plates with variable fiber spacing using the finite element method. In another research conducted by Duran et al. [22], thermal buckling analyses were performed for composite plates with spatial varying fiber orientations. Critical buckling temperature was calculated numerically using classical lamination theory and finite element method. As a result, for symmetrically balanced laminates subjected to constant thermal load, the optimum fiber path with the highest thermal buckling resistance was found for different material models.

In the research reviewed so far, studies on fiber-reinforced composite material and buckling of the composite material were examined. The researchers went a step further and examined the buckling behavior of fiber reinforced composite materials. One of these studies was done by Malekzadeh and Shojaee [23]. Researchers have derived the stability equations according to the first-order shear deformation theory of plates. Investigations were carried out according to the distribution of four different single-walled carbon nanotubes. Stability equations were discretized for arbitrary boundary conditions with the mapping differential quadrature technique. Waily [24] studied the effect of different types of reinforcement fiber and different types of resin on the critical buckling temperature.

Both numerical and theoretical calculations were made for the unidirectional and woven reinforcement composite plate, and the results were compared. In addition, the effect of fiber amount on critical buckling temperature was observed by changing the fiber volume fraction. In another study conducted by Waily et al. [25], the thermal buckling behavior of the composite plate reinforced with carbon nanoparticles was analytically investigated. Based on Eringen's nonlocal elasticity theory, Sari et al. [26] examined the buckling characteristic of functionally graded nano-plates under thermal and biaxial linearly varying forces. They compared the

accuracy of their work with the studies in the literature. A parametric study was performed by changing some constants. Based on the results obtained, they discovered that these parameters significantly influence the stability behavior of FG nano-plates. Aghazadeh et al. [27] investigated the statics, dynamics, and stability of functionally graded micro-plates subjected to mechanical and thermal loads. The effect of size effect, length scale parameter variations, and initial thermal displacements are shown in the numerical results. In articles by Alashti et al. [28], buckling analysis was performed for the functionally graded thick cylindrical shell with variable thickness. In this study, the loading type is combined external pressure and axial compression. In addition, the axisymmetric imperfection status is discussed, and its effect on buckling load is investigated. Satouri et al. [29] conducted a buckling analysis study for two dimensional functionally graded cylindrical shell reinforced with axial stiffeners. The shell studied is graded in the thickness and length direction. Equilibrium and stability equations obtained using third-order shear deformation theory are solved by the differential quadrature method. In another research, Hajlaoui et al. [30] examined the buckling behavior of functionally graded nanotube-reinforced composite shell using modified first-order enhanced solid shell element formulation. In this research, five different single-walled carbon nanotube distributions were studied. The numeric results obtained were compared with the results of other investigators, and the performance of the developed solid-shell element was observed. Shen et al. [31] developed a model to examine graphene-reinforced composite laminated plate thermal buckling behavior exposed to in-plane temperature variation. The plate foundation interaction and temperature variation effects are also reflected in the model. Governing equations are derived using higher-order shear deformation plate theory. Based on first-order shear deformation theory, Lei et al. [32] studied the buckling behavior of carbon-nanotube reinforced functionally graded composite laminated plate. The effects of rotary inertia and transverse shear deformation were understood with the theory used. In the study, Ebrahimi et al. [33] investigated the thermal buckling behavior of functionally graded nanocomposite plates reinforced with graphene oxide powder. Researchers

evaluated four different GOP's distributions and which model was the most suitable for the stability of the structure. Apart from this, the effects of different types of thermal loading, the weight fraction of GOP, and elastic foundation constants on the buckling load of the structure were studied by conducting a parametric study. In research conducted by Shen [34], the thermal buckling and post-buckling behavior of two types of fiber-reinforced laminated plates were investigated. Numerical results have been obtained for the fiber-reinforced composite plate with polymer matrix and metal matrix. According to the results, the effect of functionally graded fiber reinforcements on thermal buckling strength is more pronounced in polymer matrix plate than metal matrix plate. In all the articles reviewed, composite materials' behavior in vibration, buckling, and post-buckling has been investigated. By using different theories and material models, the theory and model that best reflects the behavior of composite structures have been obtained. Despite a lot of work on composite materials, there are still incomplete studies on some issues. As can be seen from the above studies, no studies have been conducted on the buckling behavior of graded fiber reinforcement symmetric and unsymmetric composite plate under thermal loading. Therefore, in this study, classical lamination plate theory will be used to investigate the buckling behavior of graded fiber reinforcement symmetric and unsymmetric composite plate under thermal loading, and solutions will be obtained by the differential quadrature method. By using DQM, fast, accurate analysis with shorter processing time can be made. It is used efficiently in buckling analyses involving high-order differential equations with a variable coefficient. Moreover, it is difficult to write a series solution because there are bending-twisting terms in the governing equation in the problem examined in this thesis. For this reason, DQM is preferred. The results for two boundary conditions, simply supported and clamped will be examined.

1.3 Motivation and Scope of Study

The study's main objective is to predict the buckling behavior of graded fiber-reinforced composite plates under thermal loading. In the study, it is desired to observe the effect of different parameters on the critical buckling temperature. For this reason, the results are obtained by changing the parameters. The effect of the symmetrical or unsymmetrical state of the plate on the critical buckling temperature is investigated. Also, the effect of different boundary conditions on the critical buckling temperature is investigated. Classical lamination plate theory and the differential quadrature method are used in all cases examined. In the research carried out so far, there is no study related to the buckling behavior of unsymmetric laminated composite structures under loads caused by thermal effect. This study investigates the thermal buckling behavior of unsymmetric laminated composite structures with variable fiber volume fractions for different boundary conditions. Therefore, this study is a new contribution to the literature. The organizational chart of the study is as follows.

In CHAPTER 2, the governing equations expressing the buckling behavior of graded fiber-reinforced composite materials at some boundary conditions are derived using classical laminated plate theory. Hamilton's principle is used in the derivation stage. The material properties change according to the fiber volume, and this change is seen in the thickness direction. Grading of the material has been considered in the derivation of the formulas.

In CHAPTER 3, a solution procedure is developed using DQM to solve the derived governing equations and boundary conditions together. A commercial tool, MATLAB, is used to reach the numerical solution. The solution procedure to be followed with DQM is adapted to MATLAB.

In CHAPTER 4, numerical results and parametric studies are shown. The results obtained using DQM is compared with similar studies in the literature, and the error rates is observed by plotting the results on top of each other. Also, the same problem

is modeled using Abaqus. The results obtained using DQM in MATLAB are compared with those obtained using Abaqus. Based on all the results obtained, it has been shown that the study is verified.

In CHAPTER 5, the output of the thesis is expressed, comments is made regarding the results, and information is given for future studies.

CHAPTER 2

FORMULATION

2.1 Kirchhoff Plate Theory

The geometry of the composite plate with its length, width, and thickness presented with a, b, and h, respectively, is schematically shown in Figure 2.1. The initial position and the displacement of an arbitrary point *A* located at a distance z from the mid-surface of the plate is also depicted in Figure 2.2. As it can be observed, the transverse displacement results in a corresponding in-plane displacements. Denoting the displacements of point *A* at any instant along x, y, and z directions by u, v, and w, respectively, the displacement field can be expressed as follows.

$$u(x,y,z) = u_0(x,y) - z\frac{\partial w}{\partial x} \tag{2.1}$$

$$v(x,y,z) = v_0(x,y) - z\frac{\partial w}{\partial y} \tag{2.2}$$

$$w(x,y,z) = w_0(x,y) \tag{2.3}$$

where u_0, v_0, w_0 are the displacement in the middle surface of the plate

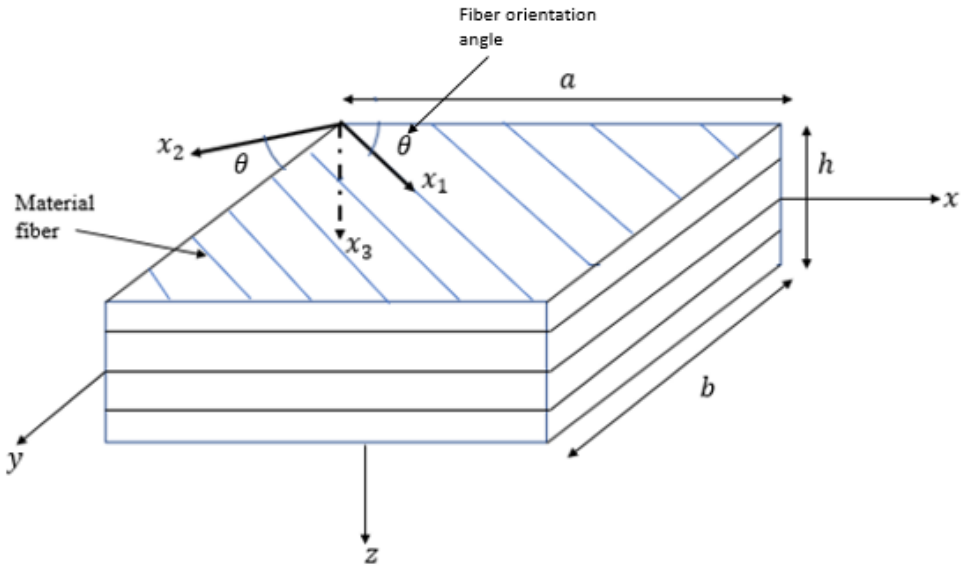

Figure 2.1. Graded fiber-reinforced composite plate

x_1, x_2, and x_3 are the material coordinates whereas x,y, and z are the general coordinates.

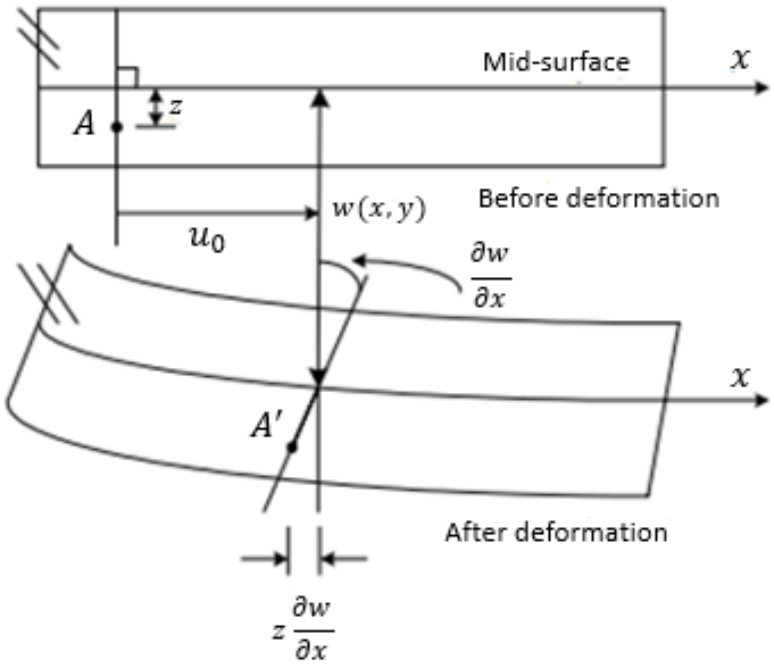

Figure 2.2. Deformed configuration of a graded fiber-reinforced plate

Note that the Kirchhoff plate theory ignores the effects of transverse shear strains [35]. The assumptions made in Kirchhoff plate theory are listed below.

- Line elements perpendicular to the middle surface of the plate before deformation remain normal and unstretched after deformation.
- The deflections of the graded fiber reinforcement composite plate are small compared to its thickness h, so the linear strain-displacement relations are valid.
- The thickness of the plate is in the range of 1/20~1/100 of its span, hence it is sufficiently low for the normal stress in the thickness direction to be neglected.

Strain equations for graded fiber-reinforced composite plate are expressed as follows.

$$\varepsilon_{xx} = \frac{\partial u}{\partial x} \tag{2.4}$$

$$\varepsilon_{xx} = \varepsilon_{x0} - z\frac{\partial^2 w}{\partial x^2} \tag{2.5}$$

$$\varepsilon_{yy} = \frac{\partial v}{\partial y} \tag{2.6}$$

$$\varepsilon_{yy} = \varepsilon_{y0} - z\frac{\partial^2 w}{\partial y^2} \tag{2.7}$$

$$\gamma_{xy} = \frac{\partial u}{\partial y} + \frac{\partial v}{\partial x} \tag{2.8}$$

$$\gamma_{xy} = \gamma_{xy0} - 2z\frac{\partial^2 w}{\partial x \partial y} \tag{2.9}$$

$$\varepsilon_{zz} = \gamma_{xz} = \gamma_{yz} = 0 \tag{2.10}$$

$$\varepsilon_{x0} = \frac{\partial u_0}{\partial x} \ , \ \varepsilon_{y0} = \frac{\partial v_0}{\partial x} \ , \ \gamma_{xy0} = \frac{\partial u_0}{\partial y} + \frac{\partial v_0}{\partial x} \tag{2.11}$$

2.2 Plane Stress Constitutive Relations

Plane stress is a condition which states that the normal stress and shear stresses perpendicular to the x-y plane are zero. The normal and shear stress components are σ_{zz}, σ_{xz} and σ_{yz}. This assumption can be utilized in analysing thin plates which possess small size in thickness direction compared to its dimensions in other directions. According to plane stress state, for a graded fiber-reinforced material the stresses are expressed in terms of strains through the following relations [40].

$$\begin{bmatrix} \sigma_1 \\ \sigma_2 \\ \tau_{12} \end{bmatrix} = \begin{bmatrix} Q_{11} & Q_{12} & 0 \\ Q_{12} & Q_{22} & 0 \\ 0 & 0 & Q_{66} \end{bmatrix} \begin{bmatrix} \varepsilon_1 - \alpha_1 \Delta T \\ \varepsilon_2 - \alpha_2 \Delta T \\ \gamma_{12} \end{bmatrix} \tag{2.12}$$

$$Q_{11}(z) = \frac{E_{11}(z)}{1 - \upsilon_{12}(z)\upsilon_{21}(z)} \tag{2.13}$$

$$Q_{12}(z) = \frac{\upsilon_{21}(z)E_{11}(z)}{1 - \upsilon_{12}(z)\upsilon_{21}(z)} \tag{2.14}$$

$$Q_{22}(z) = \frac{E_{22}(z)}{1 - \upsilon_{12}(z)\upsilon_{21}(z)} \tag{2.15}$$

$$Q_{66}(z) = G_{12}(z) \tag{2.16}$$

σ_1, σ_1, and τ_{12} correspond to stress components in material coordinate system.

ε_1, ε_1, and γ_{12} indicate strain components in material coordinate system.

α_1 and α_2 represent the thermal expansion coefficients in thex_1 and x_2 directions, respectively.

where Q_{ij} are the plane stress-reduced stiffnesses.

E_{11} and E_{22} are longitudinal and transverse Young's moduli, respectively; G_{12} denotes the in-plane shear modulus, and υ_{12}, and υ_{21} are the poisson ratios.

Since the composite plate considered in the current study is graded through the thickness, the values of Q_{ij}, E_{11}, E_{22}, G_{12}, υ_{12}, and υ_{21} depend on the z coordinate.

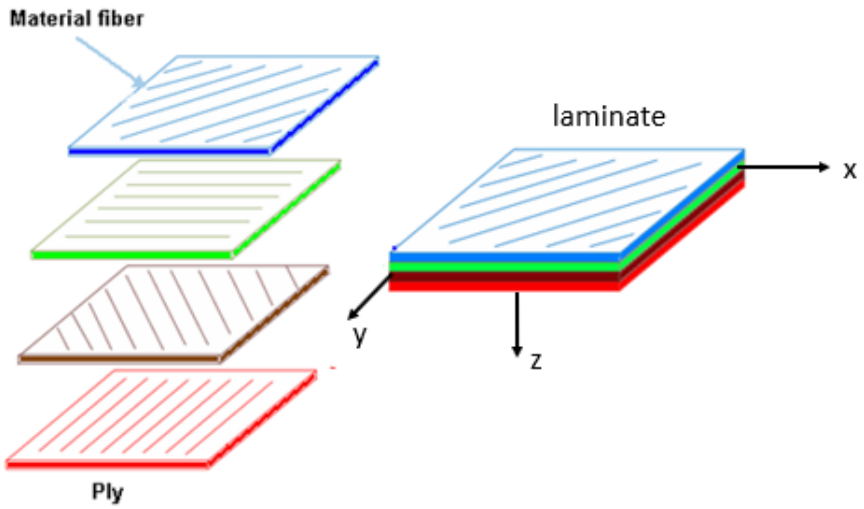

Figure 2.3. Plies orientation of composite laminate

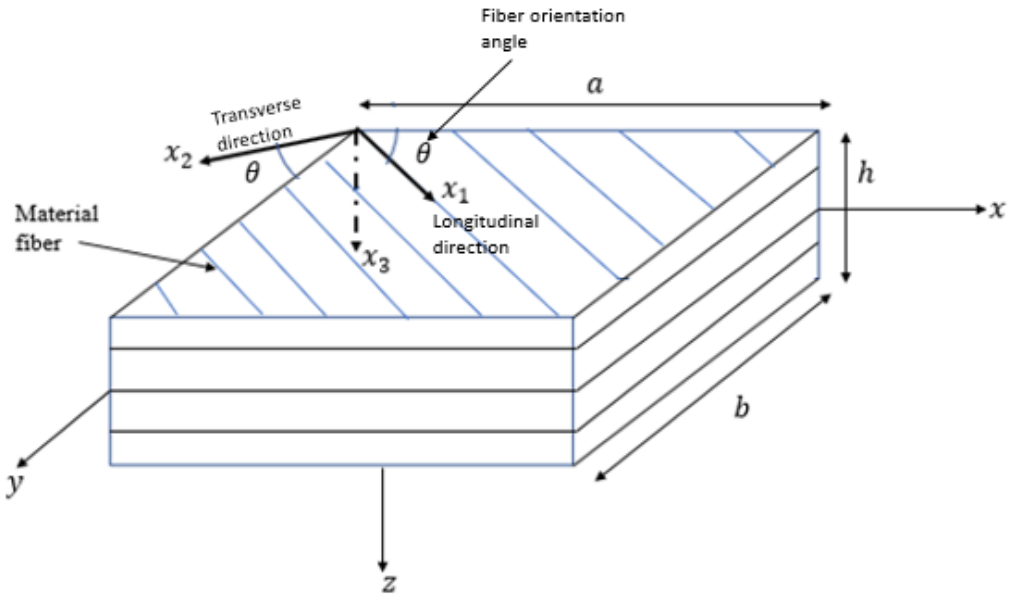

Figure 2.4. Principal direction of composite laminate

Lamina or ply is the smallest fundamental unit that makes up the laminate. The structure formed by the combination of more than one lamina to obtain the desired material properties is called laminate. Figure 2.3 shows a typical laminate and the plies forming it. The plies consist of fibers with different orientations. The fiber orientation angle is indicated by θ. The plies and fiber orientations are also shown in Figure 2.3. This sequence of angle plies is called the stacking sequence or lamination scheme. An angle ply laminate can be either symmetric or unsymmetric. If a laminate has the same material and identical lamination orientation with respect to the midsurface, it is symmetric; otherwise, it is unsymmetric. Figure 2.4 shows the longitudinal and transverse directions of the fiber-reinforced composite plate.

The ply orientations of each lamina forming the composite plate are different. Therefore, it is necessary to transform the orientations of the laminae in a single direction. The transformed stress-strain relationship of the orthotropic plate under thermal loading, according to the plane stress condition, is given below.

$$\begin{bmatrix}\sigma_{xx}\\ \sigma_{yy}\\ \sigma_{xy}\end{bmatrix}=\begin{bmatrix}\bar{Q}_{11} & \bar{Q}_{12} & \bar{Q}_{16}\\ \bar{Q}_{12} & \bar{Q}_{22} & \bar{Q}_{26}\\ \bar{Q}_{16} & \bar{Q}_{26} & \bar{Q}_{66}\end{bmatrix}\begin{bmatrix}\varepsilon_{xx}-\alpha_{xx}\Delta T\\ \varepsilon_{yy}-\alpha_{yy}\Delta T\\ \varepsilon_{xy}-\alpha_{xy}\Delta T\end{bmatrix} \quad \textbf{(2.17)}$$

σ_{xx} , σ_{yy} and σ_{xy} indicate stress components.

where α_{xx} , α_{yy}, and α_{xy} are the transformed thermal expansion coefficients [39].

$$\alpha_{xx} = \alpha_1 cos^2(\theta) + \alpha_2 sin^2(\theta) \quad \textbf{(2.18)}$$

$$\alpha_{yy} = \alpha_1 sin^2(\theta) + \alpha_2 cos^2(\theta) \quad \textbf{(2.19)}$$

$$\alpha_{xy} = (\alpha_1 - \alpha_2) sin(\theta) cos(\theta) \quad \textbf{(2.20)}$$

The stress-strain equation for the k^{th} layer of a graded fiber reinforcement composite plate with N layers is as follows.

$$[\sigma]_k = \left[\bar{Q}_{ij}\right]_k [\varepsilon]_k \tag{2.21}$$

where $\bar{Q}_{ij}$ is called the transformed plane stress-reduced stiffnesses.

$$\bar{Q}_{11}(z) = Q_{11}(z)cos^4(\theta) + 2[Q_{12}(z) + 2Q_{66}(z)]\, sin^2(\theta)cos^2(\theta) + Q_{22}(z)sin^4(\theta) \tag{2.22}$$

$$\bar{Q}_{12}(z) = [Q_{11}(z) + Q_{22}(z) - 4Q_{66}(z)]\, sin^2(\theta)cos^2(\theta) + Q_{12}(z)[sin^4(\theta) + cos^4(\theta)] \tag{2.23}$$

$$\bar{Q}_{22}(z) = Q_{11}(z)sin^4(\theta) + 2[Q_{12}(z) + 2Q_{66}(z)]\, sin^2(\theta)cos^2(\theta) + Q_{22}(z)cos^4(\theta) \tag{2.24}$$

$$\bar{Q}_{16}(z) = [Q_{11}(z) - Q_{12}(z) - 2Q_{66}(z)]\, sin(\theta)cos^3(\theta) + [Q_{12}(z) - Q_{22}(z) + 2Q_{66}(z)]\, sin^3(\theta)cos(\theta) \tag{2.25}$$

$$\bar{Q}_{26}(z) = [Q_{11}(z) - Q_{12}(z) - 2Q_{66}(z)]\, sin^3(\theta)cos(\theta) + [Q_{12}(z) - Q_{22}(z) + 2Q_{66}(z)]\, sin(\theta)cos^3(\theta) \tag{2.26}$$

$$\bar{Q}_{66}(z) = [Q_{11}(z) + Q_{22}(z) - 2Q_{12}(z) - 2Q_{66}(z)]\, sin^2(\theta)cos^2(\theta) + Q_{66}(z)[sin^4(\theta) + cos^4(\theta)] \tag{2.27}$$

2.3 Derivation of Governing Equations of Boundary Conditions Using Hamilton's Principle

In the case of buckling, kinetic energy is not considered and hence it is only needed that the strain energy variation δU to be equal to zero [39].

$$\delta U = \int_{R_0} \int_{-\frac{h}{2}}^{\frac{h}{2}} \left(\sigma_{xx}\delta\varepsilon_{xx} + \sigma_{yy}\delta\varepsilon_{yy} + 2\sigma_{xy}\delta\varepsilon_{xy}\right) dz dx dy = 0 \tag{2.28}$$

$$\delta U = \int_{R_0} \int_{-\frac{h}{2}}^{\frac{h}{2}} \Big(\sigma_{xx}\left(\delta{\varepsilon_{xx}}^0 + z\delta{\varepsilon_{xx}}^1\right) + \sigma_{yy}\left(\delta{\varepsilon_{yy}}^0 + z\delta{\varepsilon_{yy}}^1\right) + \sigma_{xy}\left(\delta{\gamma_{xy}}^0 + z\delta{\gamma_{xy}}^1\right)\Big) dz dx dy = 0 \tag{2.29}$$

$$\delta U = \int_{R_0} \left(N_{xxr} \delta {\varepsilon_{xx}}^0 + M_{xxr} \delta {\varepsilon_{xx}}^1 + N_{yyr} \delta {\varepsilon_{yy}}^0 + M_{yyr} \delta {\varepsilon_{yy}}^1 + N_{xyr} \delta {\gamma_{xy}}^0 + M_{xyr} \delta {\gamma_{xy}}^1 \right) dxdy = 0 \quad \textbf{(2.30)}$$

N_{xxr} , N_{yyr} and N_{xyr} are in-plane force resultants and M_{xxr}, M_{yyr} and M_{xyr} are the moment resultants [39].

The symbol δ is a variational operator which is used to express the variation or virtual change in a quantity $\delta {\varepsilon_{xx}}^0$, $\delta {\varepsilon_{yy}}^0$, $\delta {\varepsilon_{xy}}^0$ are the variations of membrane strains and $\delta {\varepsilon_{xx}}^1$, $\delta {\varepsilon_{yy}}^1$, $\delta {\varepsilon_{xy}}^1$ are the variations of bending strains. δU is strain energy variation.

R_0 represents the area.

The strain variations can be written in the following form [39].

$$\delta {\varepsilon_{xx}}^0 = \frac{\partial \delta u_0}{\partial x} + \frac{\partial w_0}{\partial x} \frac{\partial \delta w_0}{\partial x} \quad \textbf{(2.31)}$$

$$\delta {\varepsilon_{xx}}^1 = -\frac{\partial^2 \delta w_0}{\partial x^2} \quad \textbf{(2.32)}$$

$$\delta {\varepsilon_{yy}}^0 = \frac{\partial \delta v_0}{\partial y} + \frac{\partial w_0}{\partial y} \frac{\partial \delta w_0}{\partial y} \quad \textbf{(2.33)}$$

$$\delta {\varepsilon_{yy}}^1 = -\frac{\partial^2 \delta w_0}{\partial y^2} \quad \textbf{(2.34)}$$

$$\delta {\gamma_{xy}}^0 = \frac{\partial \delta u_0}{\partial y} + \frac{\partial \delta v_0}{\partial x} + \frac{\partial \delta w_0}{\partial x} \frac{\partial w_0}{\partial y} + \frac{\partial w_0}{\partial x} \frac{\partial \delta w_0}{\partial y} \quad \textbf{(2.35)}$$

$$\delta {\gamma_{xy}}^1 = -2 \frac{\partial^2 \delta w_0}{\partial x \partial y} \quad \textbf{(2.36)}$$

Plugging the equations (2.31) to (2.36) into equation (2.30) yields:

$$\delta U = \int_{R_0} \Big(N_{xxr,x}\delta u_0 + (N_{xxr}\frac{\partial w_0}{\partial x})_{,x}\delta w_0 + M_{xxr,xx}\delta w_0 + N_{yyr,y}\delta v_0 + (N_{yyr}\frac{\partial w_0}{\partial y})_{,y}\delta w_0 + M_{yyr,yy}\delta w_0 + N_{xyr,y}\delta u_0 + N_{xyr,x}\delta v_0 + (N_{xyr}\frac{\partial w_0}{\partial y})_{,x}\delta w_0 + (N_{xyr}\frac{\partial w_0}{\partial x})_{,y}\delta w_0 + 2M_{xyr,xy}\delta w_0 \Big) dxdy = 0 \quad \textbf{(2.37)}$$

Equation (2.34) can be rearranged in terms of virtual displacements (δu_0, δv_0, δw_0) as given below.

$$\delta U = \int_{R_0} \begin{pmatrix} (N_{xxr,x} + N_{xyr,y})\delta u_0 + \\ (N_{yyr,y} + N_{xyr,x})\delta v_0 + \\ (M_{xxr,xx} + 2M_{xyr,xy} + M_{yyr,yy} + N(w_0))\delta w_0 \end{pmatrix} dxdy = 0 \quad \textbf{(2.38)}$$

$$\mathrm{N}(w_0) = \frac{\partial}{\partial x}(N_{xxr}\frac{\partial w_0}{\partial x} + N_{xyr}\frac{\partial w_0}{\partial y}) + \frac{\partial}{\partial y}(N_{xyr}\frac{\partial w_0}{\partial x} + N_{yyr}\frac{\partial w_0}{\partial y}) \quad \textbf{(2.39)}$$

Resultant force consists of mechanic and thermal parts. Mechanic part exists for state of stability and thermal part exists for state of equilibrium condition. $N(w_0)$ consists of prebuckling thermal force resultants [42]. Therefore, $N(w_0)$ is expressed as.

$$N(w_0) = \frac{\partial w_0}{\partial x}\left(\frac{\partial \bar{N}_{xx}{}^T}{\partial x} + \frac{\partial \bar{N}_{xy}{}^T}{\partial y}\right) + \frac{\partial w_0}{\partial y}\left(\frac{\partial \bar{N}_{xy}{}^T}{\partial x} + \frac{\partial \bar{N}_{yy}{}^T}{\partial y}\right) + \bar{N}_{xx}{}^T\frac{\partial^2 w_0}{\partial x^2} + 2\bar{N}_{xy}{}^T\frac{\partial^2 w_0}{\partial x \partial y} + \bar{N}_{yy}{}^T\frac{\partial^2 w_0}{\partial y^2} \quad \textbf{(2.40)}$$

Since the force resulting from the thermal effect is constant, the derivative of these force with respect to x and y is zero. Therefore, the equation in (2.40) becomes as follows.

$$N(w_0) = \bar{N}_{xx}{}^T\frac{\partial^2 w_0}{\partial x^2} + 2\bar{N}_{xy}{}^T\frac{\partial^2 w_0}{\partial x \partial y} + \bar{N}_{yy}{}^T\frac{\partial^2 w_0}{\partial y^2} \quad \textbf{(2.41)}$$

Since $\bar{N}_{xy}{}^{T} = 0$

$$N(w_0) = \bar{N}_{xx}{}^{T}\frac{\partial^2 w_0}{\partial x^2} + \bar{N}_{yy}{}^{T}\frac{\partial^2 w_0}{\partial y^2} \tag{2.42}$$

The Euler-Lagrange equations of the theory are obtained when the coefficients of each virtual displacements $(\delta u_0, \delta v_0, \delta w_0)$ are individually set to zero [39].

$$N_{xxr,x} + N_{xyr,y} = 0 \tag{2.43}$$

$$N_{yyr,y} + N_{xyr,x} = 0 \tag{2.44}$$

$$M_{xxr,xx} + 2M_{xyr,xy} + M_{yyr,yy} + N(w_0) = 0 \tag{2.45}$$

Equations (2.43)-(2.45) contain force and moment terms which are given by the following expressions.

$$\begin{bmatrix} N_{xxr} \\ N_{yyr} \\ N_{xyr} \end{bmatrix} = \sum_{k=1}^{N}\int_{z_k}^{z_{k+1}} \begin{bmatrix} \sigma_{xx} \\ \sigma_{yy} \\ \sigma_{xy} \end{bmatrix} dz = \begin{bmatrix} N_{xx} \\ N_{yy} \\ N_{xy} \end{bmatrix} - \begin{bmatrix} \bar{N}_{xx}{}^{T} \\ \bar{N}_{yy}{}^{T} \\ \bar{N}_{xy}{}^{T} \end{bmatrix} \tag{2.46}$$

where subscript *r* stands for resultants, and N_{xxr} , N_{yyr} , and N_{xyr} are the resultant forces. superscript *T* indicates thermal effects. As it can be seen from equation (2.46), the resultant forces are comprised of mechanical forces N_{xx} , N_{yy} , and N_{xy}, and thermal forces $\bar{N}_{xx}{}^{T}$, $\bar{N}_{yy}{}^{T}$, and $\bar{N}_{xy}{}^{T}$. These forces are defined as follows.

$$\begin{bmatrix} N_{xx} \\ N_{yy} \\ N_{xy} \end{bmatrix} = \sum_{k=1}^{N}\int_{z_k}^{z_{k+1}} \begin{bmatrix} \bar{Q}_{11} & \bar{Q}_{12} & \bar{Q}_{16} \\ \bar{Q}_{12} & \bar{Q}_{22} & \bar{Q}_{26} \\ \bar{Q}_{16} & \bar{Q}_{26} & \bar{Q}_{66} \end{bmatrix}^{k} \begin{bmatrix} \varepsilon_{x0} - z\dfrac{\partial^2 w_0}{\partial x^2} \\ \varepsilon_{y0} - z\dfrac{\partial^2 w_0}{\partial y^2} \\ \varepsilon_{xy0} - 2z\dfrac{\partial^2 w_0}{\partial x \partial y} \end{bmatrix} dz \tag{2.47}$$

$$\begin{bmatrix} N_{xx} \\ N_{yy} \\ N_{xy} \end{bmatrix} = \begin{bmatrix} A_{11} & A_{12} & A_{16} \\ A_{12} & A_{22} & A_{26} \\ A_{16} & A_{26} & A_{66} \end{bmatrix} \begin{bmatrix} \varepsilon_{x0} \\ \varepsilon_{y0} \\ \varepsilon_{xy0} \end{bmatrix} + \begin{bmatrix} B_{11} & B_{12} & B_{16} \\ B_{12} & B_{22} & B_{26} \\ B_{16} & B_{26} & B_{66} \end{bmatrix} \begin{bmatrix} -\frac{\partial^2 w}{\partial x^2} \\ -\frac{\partial^2 w}{\partial y^2} \\ -2\frac{\partial^2 w}{\partial x \partial y} \end{bmatrix} \quad \textbf{(2.48)}$$

$$\begin{bmatrix} \bar{N}_{xx}{}^T \\ \bar{N}_{yy}{}^T \\ \bar{N}_{xy}{}^T \end{bmatrix} = \sum_{k=1}^{N} \int_{z_k}^{z_{k+1}} \begin{bmatrix} A_x \\ A_y \\ A_{xy} \end{bmatrix}_k \Delta T dz = \sum_{k=1}^{N} \begin{bmatrix} A_x \\ A_y \\ A_{xy} \end{bmatrix}_k (z_{k+1} - z_k)\Delta T \quad \textbf{(2.49)}$$

The resultant moments can also be written as.

$$\begin{bmatrix} M_{xxr} \\ M_{yyr} \\ M_{xyr} \end{bmatrix} = \sum_{k=1}^{N} \int_{z_k}^{z_{k+1}} \begin{bmatrix} \sigma_{xx} \\ \sigma_{yy} \\ \sigma_{xy} \end{bmatrix} z\, dz = \begin{bmatrix} M_{xx} \\ M_{yy} \\ M_{xy} \end{bmatrix} - \begin{bmatrix} \bar{M}_{xx}{}^T \\ \bar{M}_{yy}{}^T \\ \bar{M}_{xy}{}^T \end{bmatrix} \quad \textbf{(2.50)}$$

where M_{xx} , M_{yy} , and M_{xy} are the mechanical and $\bar{M}_x{}^T$, $\bar{M}_x{}^T$, and $\bar{M}_{xy}{}^T$ are the thermal parts of resultant moments, which can be given by the following relations.

$$\begin{bmatrix} M_{xx} \\ M_{yy} \\ M_{xy} \end{bmatrix} = \sum_{k=1}^{N} \int_{z_k}^{z_{k+1}} \begin{bmatrix} \bar{Q}_{11} & \bar{Q}_{12} & \bar{Q}_{16} \\ \bar{Q}_{12} & \bar{Q}_{22} & \bar{Q}_{26} \\ \bar{Q}_{16} & \bar{Q}_{26} & \bar{Q}_{66} \end{bmatrix}^k \begin{bmatrix} \varepsilon_{x0} - z\frac{\partial^2 w}{\partial x^2} \\ \varepsilon_{y0} - z\frac{\partial^2 w}{\partial y^2} \\ \varepsilon_{xy0} - 2z\frac{\partial^2 w}{\partial x \partial y} \end{bmatrix} z\, dz \quad \textbf{(2.51)}$$

$$\begin{bmatrix} M_{xx} \\ M_{yy} \\ M_{xy} \end{bmatrix} = \begin{bmatrix} B_{11} & B_{12} & B_{16} \\ B_{12} & B_{22} & B_{26} \\ B_{16} & B_{26} & B_{66} \end{bmatrix} \begin{bmatrix} \varepsilon_{x0} \\ \varepsilon_{y0} \\ \varepsilon_{xy0} \end{bmatrix} + \begin{bmatrix} D_{11} & D_{12} & D_{16} \\ D_{12} & D_{22} & D_{26} \\ D_{16} & D_{26} & D_{66} \end{bmatrix} \begin{bmatrix} -\frac{\partial^2 w}{\partial x^2} \\ -\frac{\partial^2 w}{\partial y^2} \\ -2\frac{\partial^2 w}{\partial x \partial y} \end{bmatrix} \quad \textbf{(2.52)}$$

$$\begin{bmatrix} \bar{M}_{xx}{}^T \\ \bar{M}_{yy}{}^T \\ \bar{M}_{xy}{}^T \end{bmatrix} = \sum_{k=1}^{N} \int_{z_k}^{z_{k+1}} \begin{bmatrix} A_x \\ A_y \\ A_{xy} \end{bmatrix}_k z\Delta T dz = \frac{1}{2} \sum_{k=1}^{N} \begin{bmatrix} A_x \\ A_y \\ A_{xy} \end{bmatrix}_k ({z_{k+1}}^2 - {z_k}^2)\Delta T \quad \textbf{(2.53)}$$

where A_{ij} are called extensional stiffnesses ,D_{ij} bending stiffnesses , B_{ij} bending extensional coupling stiffnesses [1].

A_x, A_y , and A_{xy} are known as thermal stiffnesses [1].

$$A_{ij} = \int_{-\frac{h}{2}}^{\frac{h}{2}} \bar{Q}_{ij}\, dz = \sum_{k=1}^{N} \bar{Q}_{ij}{}^{(k)} (z_{k+1} - z_k) \tag{2.54}$$

$$B_{ij} = \int_{-\frac{h}{2}}^{\frac{h}{2}} \bar{Q}_{ij}\, z\, dz = \frac{1}{2} \sum_{k=1}^{N} \bar{Q}_{ij}{}^{(k)} ({z_{k+1}}^2 - {z_k}^2) \tag{2.55}$$

$$D_{ij} = \int_{-\frac{h}{2}}^{\frac{h}{2}} \bar{Q}_{ij}\, z^2\, dz = \frac{1}{3} \sum_{k=1}^{N} \bar{Q}_{ij}{}^{(k)} ({z_{k+1}}^3 - {z_k}^3) \tag{2.56}$$

$$\begin{bmatrix} A_x \\ A_y \\ A_{xy} \end{bmatrix}_k = \begin{bmatrix} \bar{Q}_{11} & \bar{Q}_{12} & \bar{Q}_{16} \\ \bar{Q}_{12} & \bar{Q}_{22} & \bar{Q}_{26} \\ \bar{Q}_{16} & \bar{Q}_{26} & \bar{Q}_{66} \end{bmatrix}_k \begin{bmatrix} \cos^2(\theta) & \sin^2(\theta) \\ \sin^2(\theta) & \cos^2(\theta) \\ 2\sin(\theta)\cos(\theta) & -2\sin(\theta)\cos(\theta) \end{bmatrix}_k \begin{bmatrix} \alpha_1 \\ \alpha_2 \end{bmatrix}_k \tag{2.57}$$

According to the equations in (2.43) and (2.44), the following equations are obtained.

$$N_{xxr,x} + N_{xyr,y} = N_{xx,x} + N_{xy,y} + \bar{N}_{xx,x}{}^T + \bar{N}_{xy,y}{}^T = 0 \tag{2.58}$$

$$N_{yyr,y} + N_{xyr,x} = N_{yy,y} + N_{xy,x} + \bar{N}_{yy,y}{}^T + \bar{N}_{xy,x}{}^T = 0 \tag{2.59}$$

Since the force resulting from the thermal effect is constant, the derivative of this force with respect to x and y is zero. Consequently, the equations (2.58) and (2.59) recast into the following form.

$$N_{xxr,x} + N_{xyr,y} = N_{xx,x} + N_{xy,y} = 0 \tag{2.60}$$

$$N_{yyr,y} + N_{xyr,x} = N_{yy,y} + N_{xy,x} = 0 \tag{2.61}$$

Similarly, by the aid of equation (2.50),equation (2.45) is expanded as follows.

$$\begin{aligned} &M_{xxr,xx} + 2M_{xyr,xy} + M_{yyr,yy} + N(w_0) \\ &\quad = M_{xx,xx} + 2M_{xy,xy} + M_{yy,yy} + \bar{M}_{xx,xx}{}^T + 2\bar{M}_{xy,xy}{}^T \\ &\quad + \bar{M}_{yy,yy}{}^T + N(w_0) = 0 \end{aligned} \tag{2.62}$$

Since the moment resulting from the thermal effect is constant, the derivative of this moment with respect to x and y is zero. Therefore, the equation in (2.62) turns into equation (2.63).

$$\begin{aligned} &\mathrm{M_{xxr,xx}} + 2\mathrm{M_{xyr,xy}} + \mathrm{M_{yyr,yy}} + \mathrm{N}(\mathrm{w_0}) \\ &\qquad = \mathrm{M_{xx,xx}} + 2\mathrm{M_{xy,xy}} + \mathrm{M_{yy,yy}} + \mathrm{N}(\mathrm{w_0}) = 0 \end{aligned} \tag{2.63}$$

Equations (2.60), (2.61) , and (2.63) are the three equations governing the buckling problem of fiber-reinforced laminated composite plates.

Using equation (2.48), the forcing terms appeared in equations (2.60) and (2.61) are related to displacements through the relations given below.

$$\begin{aligned} N_{xx} = {} & A_{11}\frac{\partial u_0}{\partial x} + A_{12}\frac{\partial v_0}{\partial y} + A_{16}\left(\frac{\partial u_0}{\partial y} + \frac{\partial v_0}{\partial x}\right) \\ & - \left(B_{11}\frac{\partial^2 w_0}{\partial x^2} + B_{12}\frac{\partial^2 w_0}{\partial y^2} + 2B_{16}\frac{\partial^2 w_0}{\partial x \partial y}\right) \end{aligned} \tag{2.64}$$

$$\begin{aligned} N_{yy} = {} & A_{12}\frac{\partial u_0}{\partial x} + A_{22}\frac{\partial v_0}{\partial y} + A_{26}\left(\frac{\partial u_0}{\partial y} + \frac{\partial v_0}{\partial x}\right) \\ & - \left(B_{12}\frac{\partial^2 w_0}{\partial x^2} + B_{22}\frac{\partial^2 w_0}{\partial y^2} + 2B_{26}\frac{\partial^2 w_0}{\partial x \partial y}\right) \end{aligned} \tag{2.65}$$

$$\begin{aligned} N_{xy} = {} & A_{16}\frac{\partial u_0}{\partial x} + A_{26}\frac{\partial v_0}{\partial y} + A_{66}\left(\frac{\partial u_0}{\partial y} + \frac{\partial v_0}{\partial x}\right) \\ & - \left(B_{16}\frac{\partial^2 w_0}{\partial x^2} + B_{26}\frac{\partial^2 w_0}{\partial y^2} + 2B_{66}\frac{\partial^2 w_0}{\partial x \partial y}\right) \end{aligned} \tag{2.66}$$

$$\begin{aligned} N_{xx,x} = {} & A_{11}\frac{\partial^2 u_0}{\partial x^2} + A_{12}\frac{\partial^2 v_0}{\partial x \partial y} + A_{16}\left(\frac{\partial^2 u_0}{\partial x \partial y} + \frac{\partial^2 v_0}{\partial x^2}\right) \\ & - \left(B_{11}\frac{\partial^3 w_0}{\partial x^3} + B_{12}\frac{\partial^3 w_0}{\partial y^2 \partial x} + 2B_{16}\frac{\partial^3 w_0}{\partial x^2 \partial y}\right) \end{aligned} \tag{2.67}$$

$$N_{xy,y} = A_{16}\frac{\partial^2 u_0}{\partial x \partial y} + A_{26}\frac{\partial^2 v_0}{\partial y^2} + A_{66}\left(\frac{\partial^2 u_0}{\partial y^2} + \frac{\partial^2 v_0}{\partial x \partial y}\right) - \left(B_{16}\frac{\partial^3 w_0}{\partial x^2 \partial y} + B_{26}\frac{\partial^3 w_0}{\partial y^3} + 2B_{66}\frac{\partial^3 w_0}{\partial x \partial y^2}\right) \quad \textbf{(2.68)}$$

$$N_{yy,y} = A_{12}\frac{\partial^2 u_0}{\partial x \partial y} + A_{22}\frac{\partial^2 v_0}{\partial y^2} + A_{26}\left(\frac{\partial^2 u_0}{\partial y^2} + \frac{\partial^2 v_0}{\partial x \partial y}\right) - \left(B_{12}\frac{\partial^3 w_0}{\partial x^2 \partial y} + B_{22}\frac{\partial^3 w_0}{\partial y^3} + 2B_{26}\frac{\partial^3 w_0}{\partial x \partial y^2}\right) \quad \textbf{(2.69)}$$

$$N_{xy,x} = A_{16}\frac{\partial^2 u_0}{\partial x^2} + A_{26}\frac{\partial^2 v_0}{\partial x \partial y} + A_{66}\left(\frac{\partial^2 u_0}{\partial x \partial y} + \frac{\partial^2 v_0}{\partial x^2}\right) - \left(B_{16}\frac{\partial^3 w_0}{\partial x^3} + B_{26}\frac{\partial^3 w_0}{\partial y^2 \partial x} + 2B_{66}\frac{\partial^3 w_0}{\partial y \partial x^2}\right) \quad \textbf{(2.70)}$$

When the equations (2.67) and (2.68) are plugged into the equation (2.60), the following equation is obtained.

$$A_{11}\frac{\partial^2 u_0}{\partial x^2} + 2A_{16}\frac{\partial^2 u_0}{\partial x \partial y} + A_{66}\frac{\partial^2 u_0}{\partial y^2} + A_{16}\frac{\partial^2 v_0}{\partial x^2} + (A_{12} + A_{66})\frac{\partial^2 v_0}{\partial x \partial y} + A_{26}\frac{\partial^2 v_0}{\partial y^2} - \left(B_{11}\frac{\partial^3 w_0}{\partial x^3} + 3B_{16}\frac{\partial^3 w_0}{\partial x^2 \partial y} + (B_{12} + 2B_{66})\frac{\partial^3 w_0}{\partial y^2 \partial x} + B_{26}\frac{\partial^3 w_0}{\partial y^3}\right) = 0 \quad \textbf{(2.71)}$$

By plugging the equations (2.69) to (2.70) into the equation (2.61) , the equation in (2.72) can be reached.

$$A_{16}\frac{\partial^2 u_0}{\partial x^2} + (A_{12} + A_{66})\frac{\partial^2 u_0}{\partial x \partial y} + A_{26}\frac{\partial^2 u_0}{\partial y^2} + A_{22}\frac{\partial^2 v_0}{\partial y^2} + 2A_{26}\frac{\partial^2 v_0}{\partial x \partial y} + A_{66}\frac{\partial^2 v_0}{\partial x^2} - \left(B_{16}\frac{\partial^3 w_0}{\partial x^3} + (B_{12} + 2B_{66})\frac{\partial^3 w_0}{\partial x^2 \partial y} + 3B_{26}\frac{\partial^3 w_0}{\partial x \partial y^2} + B_{22}\frac{\partial^3 w_0}{\partial y^3}\right) = 0 \quad \textbf{(2.72)}$$

Using the equation in (2.52), the moment equations for a composite plate can be written as follows.

$$M_{xx} = B_{11}\frac{\partial u_0}{\partial x} + B_{12}\frac{\partial v_0}{\partial y} + B_{16}\left(\frac{\partial u_0}{\partial y} + \frac{\partial v_0}{\partial x}\right) - \left(D_{11}\frac{\partial^2 w_0}{\partial x^2} + D_{12}\frac{\partial^2 w_0}{\partial y^2} + 2D_{16}\frac{\partial^2 w_0}{\partial x \partial y}\right) \quad \textbf{(2.73)}$$

$$M_{yy} = B_{12}\frac{\partial u_0}{\partial x} + B_{22}\frac{\partial v_0}{\partial y} + B_{26}\left(\frac{\partial u_0}{\partial y} + \frac{\partial v_0}{\partial x}\right) - \left(D_{12}\frac{\partial^2 w_0}{\partial x^2} + D_{22}\frac{\partial^2 w_0}{\partial y^2} + 2D_{26}\frac{\partial^2 w_0}{\partial x \partial y}\right) \quad \textbf{(2.74)}$$

$$M_{xy} = B_{16}\frac{\partial u_0}{\partial x} + B_{26}\frac{\partial v_0}{\partial y} + B_{66}\left(\frac{\partial u_0}{\partial y} + \frac{\partial v_0}{\partial x}\right) - \left(D_{16}\frac{\partial^2 w_0}{\partial x^2} + D_{26}\frac{\partial^2 w_0}{\partial y^2} + 2D_{66}\frac{\partial^2 w_0}{\partial x \partial y}\right) \quad \textbf{(2.75)}$$

$$\mathrm{M_{xx,xx}} = \mathrm{B_{11}}\frac{\partial^3 \mathrm{u_0}}{\partial \mathrm{x}^3} + \mathrm{B_{12}}\frac{\partial^3 \mathrm{v_0}}{\partial \mathrm{y}\,\partial \mathrm{x}^2} + \mathrm{B_{16}}\left(\frac{\partial^3 \mathrm{u_0}}{\partial \mathrm{y}\,\partial \mathrm{x}^2} + \frac{\partial^3 \mathrm{v_0}}{\partial \mathrm{x}^3}\right) - \left(\mathrm{D_{11}}\frac{\partial^4 w_0}{\partial \mathrm{x}^4} + \mathrm{D_{12}}\frac{\partial^4 w_0}{\partial \mathrm{y}^2\,\partial \mathrm{x}^2} + 2\mathrm{D_{16}}\frac{\partial^4 w_0}{\partial \mathrm{y}\,\partial \mathrm{x}^3}\right) \quad \textbf{(2.76)}$$

$$M_{yy,yy} = B_{12}\frac{\partial^3 u_0}{\partial x \partial y^2} + B_{22}\frac{\partial^3 v_0}{\partial y^3} + B_{26}\left(\frac{\partial^3 u_0}{\partial y^3} + \frac{\partial^3 v_0}{\partial x \partial y^2}\right) - \left(D_{12}\frac{\partial^4 w_0}{\partial x^2 \partial y^2} + D_{22}\frac{\partial^4 w_0}{\partial y^4} + 2D_{26}\frac{\partial^4 w_0}{\partial x \partial y^3}\right) \quad \textbf{(2.77)}$$

$$M_{xy,xy} = B_{16}\frac{\partial^3 u_0}{\partial y \partial x^2} + B_{26}\frac{\partial^3 v_0}{\partial x \partial y^2} + B_{66}\left(\frac{\partial^3 u_0}{\partial x \partial y^2} + \frac{\partial^3 v_0}{\partial y \partial x^2}\right) - \left(D_{16}\frac{\partial^4 w_0}{\partial x^3 \partial y} + D_{26}\frac{\partial^4 w_0}{\partial y^3 \partial x} + 2D_{66}\frac{\partial^4 w_0}{\partial x^2 \partial y^2}\right) \quad \textbf{(2.78)}$$

By plugging the equations (2.76) to (2.78) , and (2.42) into the equation (2.63), equation (2.79) can be obtained.

$$B_{11}\frac{\partial^3 u_0}{\partial x^3}+3B_{16}\frac{\partial^3 u_0}{\partial y\partial x^2}+(B_{12}+2B_{66})\frac{\partial^3 u_0}{\partial x\partial y^2}+B_{26}\frac{\partial^3 u_0}{\partial y^3}+B_{16}\frac{\partial^3 v_0}{\partial x^3}$$
$$+(B_{12}+2B_{66})\frac{\partial^3 v_0}{\partial y\partial x^2}+3B_{26}\frac{\partial^3 v_0}{\partial x\partial y^2}+B_{22}\frac{\partial^3 v_0}{\partial y^3}$$
$$-\left[D_{11}\frac{\partial^4 w_0}{\partial x^4}+2(D_{12}+2D_{66})\frac{\partial^4 w_0}{\partial x^2\partial y^2}+4D_{16}\frac{\partial^4 w_0}{\partial x^3\partial y}\right.$$
$$\left.+4D_{26}\frac{\partial^4 w_0}{\partial x\partial y^3}+D_{22}\frac{\partial^4 w_0}{\partial y^4}\right]+\bar{N}_{xx}{}^{T}\frac{\partial^2 w_0}{\partial x^2}+\bar{N}_{yy}{}^{T}\frac{\partial^2 w_0}{\partial y^2}=0 \quad \textbf{(2.79)}$$

The three equations given below are coupled equations [43]. These equations form the governing equation [10]. To reach the solution, these three equations must be solved together.

$$A_{11}\frac{\partial^2 u_0}{\partial x^2}+2A_{16}\frac{\partial^2 u_0}{\partial x\partial y}+A_{66}\frac{\partial^2 u_0}{\partial y^2}+A_{16}\frac{\partial^2 v_0}{\partial x^2}+(A_{12}+A_{66})\frac{\partial^2 v_0}{\partial x\partial y}$$
$$+A_{26}\frac{\partial^2 v_0}{\partial y^2}$$
$$-\left(B_{11}\frac{\partial^3 w_0}{\partial x^3}+3B_{16}\frac{\partial^3 w_0}{\partial x^2\partial y}+(B_{12}+2B_{66})\frac{\partial^3 w_0}{\partial y^2\partial x}\right.$$
$$\left.+B_{26}\frac{\partial^3 w_0}{\partial y^3}\right)=0 \quad \textbf{(2.80)}$$

$$A_{16}\frac{\partial^2 u_0}{\partial x^2}+(A_{12}+A_{66})\frac{\partial^2 u_0}{\partial x\partial y}+A_{26}\frac{\partial^2 u_0}{\partial y^2}+A_{22}\frac{\partial^2 v_0}{\partial y^2}+2A_{26}\frac{\partial^2 v_0}{\partial x\partial y}$$
$$+A_{66}\frac{\partial^2 v_0}{\partial x^2}$$
$$-\left(B_{16}\frac{\partial^3 w_0}{\partial x^3}+(B_{12}+2B_{66})\frac{\partial^3 w_0}{\partial x^2\partial y}+3B_{26}\frac{\partial^3 w_0}{\partial x\partial y^2}\right.$$
$$\left.+B_{22}\frac{\partial^3 w_0}{\partial y^3}\right)=0 \quad \textbf{(2.81)}$$

$$B_{11}\frac{\partial^3 u_0}{\partial x^3}+3B_{16}\frac{\partial^3 u_0}{\partial y\partial x^2}+(B_{12}+2B_{66})\frac{\partial^3 u_0}{\partial x\partial y^2}+B_{26}\frac{\partial^3 u_0}{\partial y^3}+B_{16}\frac{\partial^3 v_0}{\partial x^3}$$
$$+(B_{12}+2B_{66})\frac{\partial^3 v_0}{\partial y\partial x^2}+3B_{26}\frac{\partial^3 v_0}{\partial x\partial y^2}+B_{22}\frac{\partial^3 v_0}{\partial y^3}$$
$$-\left[D_{11}\frac{\partial^4 w_0}{\partial x^4}+2(D_{12}+2D_{66})\frac{\partial^4 w_0}{\partial x^2\partial y^2}+4D_{16}\frac{\partial^4 w_0}{\partial x^3\partial y}\right. \quad \textbf{(2.82)}$$
$$\left.+4D_{26}\frac{\partial^4 w_0}{\partial x\partial y^3}+D_{22}\frac{\partial^4 w_0}{\partial y^4}\right]+\bar{N}_{xx}{}^{T}\frac{\partial^2 w_0}{\partial x^2}+\bar{N}_{yy}{}^{T}\frac{\partial^2 w_0}{\partial y^2}$$
$$=0$$

In-plane compressive loads occurred due to thermal effects, which cause buckling, is shown in Figure 2.5. Effect of this loading is examined on stability. These loads are presented in governing equation as $\bar{N}_{xx}{}^{T}$ and $\bar{N}_{yy}{}^{T}$. They are expressed in equation (2.49).

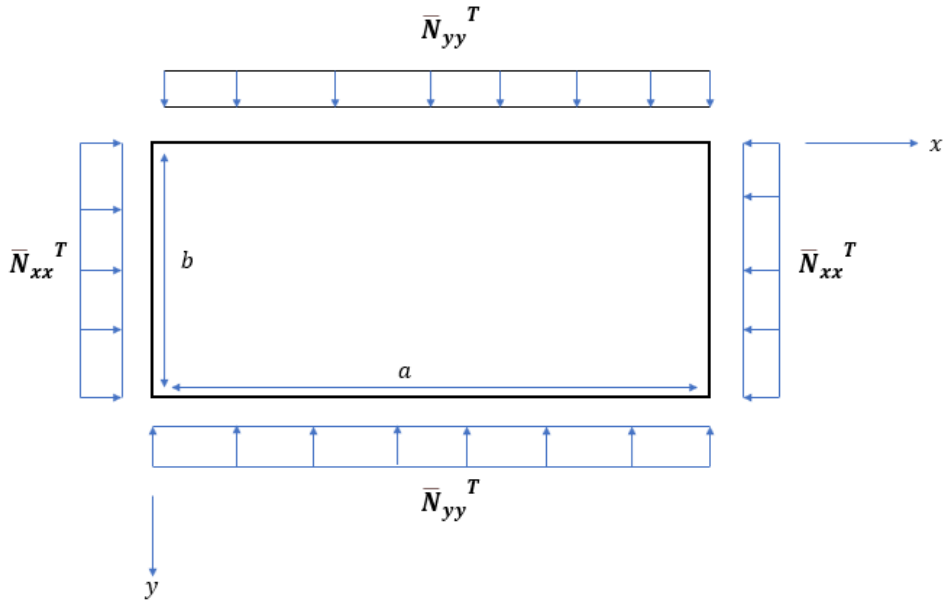

Figure 2.5. In-plane compressive forces due to thermal effects

The boundary conditions associated with all edges being simply supported [10] are expressed in (2.83) and (2.84).

$$x = 0, a; \quad u = v = w = 0; \quad M_{xx} = 0 \tag{2.83}$$

$$y = 0, b; \quad u = v = w = 0; \quad M_{yy} = 0 \tag{2.84}$$

The boundary conditions associated with all edges being clamped [17] are written below.

$$x = 0, a; \quad u = v = w = 0; \quad \frac{\partial w}{\partial x} = 0 \tag{2.85}$$

$$y = 0, b; \quad u = v = w = 0; \quad \frac{\partial w}{\partial y} = 0 \tag{2.86}$$

CHAPTER 3

NUMERICAL SOLUTION

In this study, the governing equation and boundary conditions will be solved together by a numerical method. Differential Quadrature Method will be used. This method was proposed by Bellman [36] and his co-workers in the 1970s. Generally, Differential Quadrature Method is used in boundary value problems and to solve partial differential equations. The advantage of this method is that accurate solutions can be obtained within a short period of time.

3.1 Differential Quadrature Method

Differential Quadrature Method is a discretization method that allows to find the partial derivative of the function at a point with respect to a variable. Using this method, the derivative of the function at a point can be approximated by summing the linearly weighted effect of other points on the points in that domain. Derivative of a function at a point is calculated by the differential quadrature method as in equation (3.1).

$$\frac{\partial^n f(x_i)}{\partial x^n} = A_{ij}^{(n)} f(x_j) \quad \text{and} \quad \frac{\partial^n f(y_i)}{\partial y^n} = B_{ij}^{(n)} f(y_j) \tag{3.1}$$

where $A_{ij}^{(n)}$ are called the weighting coefficients of the n^{th} derivative.

$B_{ij}^{(n)}$ are called the weighting coefficients of the n^{th} derivative and they can be found like $A_{ij}^{(n)}$.

x_i, y_i are a set of discrete points in the x ,and y direction respectively.

The weighting coefficients and the distribution of the grid points are of great importance for the accuracy of the results obtained from the differential quadrature

method. To calculate the weighting coefficients, the test function should be used to approximate the examined function. Lagrange interpolation polynomial is used as the test function. The weighting coefficients are obtained like written below [41].

$$A_{ij}^{(1)} = \frac{M^{(1)}(x_i)}{(x_i - x_j)M^{(1)}(x_j)} \quad i \neq j \quad i,j = 1,2 \ldots . N \qquad A_{ii}^{(1)} = -\sum_{j=1, i\neq j}^{N} A_{ij}^{(1)} \tag{3.2}$$

$$A_{ij}^{(2)} = \sum_{k=1}^{N} A_{ik}^{(1)} A_{kj}^{(1)} \quad \text{for } i,j = 1,2, \ldots ., N \tag{3.3}$$

$$A_{ij}^{(3)} = \sum_{k=1}^{N} A_{ik}^{(1)} A_{kj}^{(2)} \quad \text{for } i,j = 1,2, \ldots ., N \tag{3.4}$$

$$A_{ij}^{(4)} = \sum_{k=1}^{N} A_{ik}^{(1)} A_{kj}^{(3)} \quad \text{for } i,j = 1,2, \ldots ., N \tag{3.5}$$

$$\mathrm{M}(x) = \prod_{j=1}^{N}(x - x_j) \quad , \quad M^{(1)}(x_i) = \frac{\partial M(x_i)}{\partial x} = \prod_{j=1, i\neq j}^{N}(x_i - x_j) \tag{3.6}$$

N is called the number of sampling points ,and $M^{(1)}$ is Lagrangian interpolation shape function.

There are four different grid point sets for DQM which are Legendre grid points, Chebyshev grid points, Chebyshev -Gauss -Lobatto grid points , and Uniform grid points. Unequally spaced sampling points are used to obtain more accurate results in DQM. The most used sampling points in the DQM are Gauss-Lobatto-Chebyshev points. These points can be calculated by using equation (3.7).

$$x_i = \frac{1 - \cos\left(((i-1)\pi)/(N-1)\right)}{2} \tag{3.7}$$

y_i can be calculated like x_i as in equation (3.7).

3.2 Buckling

The effect that causes buckling on the structure is the thermal forces that occur due to the temperature difference in the structure. The resulting thermal in-plane loads initiate the deterioration of the stability of the structure after a certain value. The minimum load that causes buckling is called critical buckling load, and the

temperature is called critical buckling temperature. When the governing equation and boundary conditions are combined, a set of linear equations are formed. Eigenvalue can be found by solving the linear equations set. The eigenvalue is equal to critical buckling temperature.

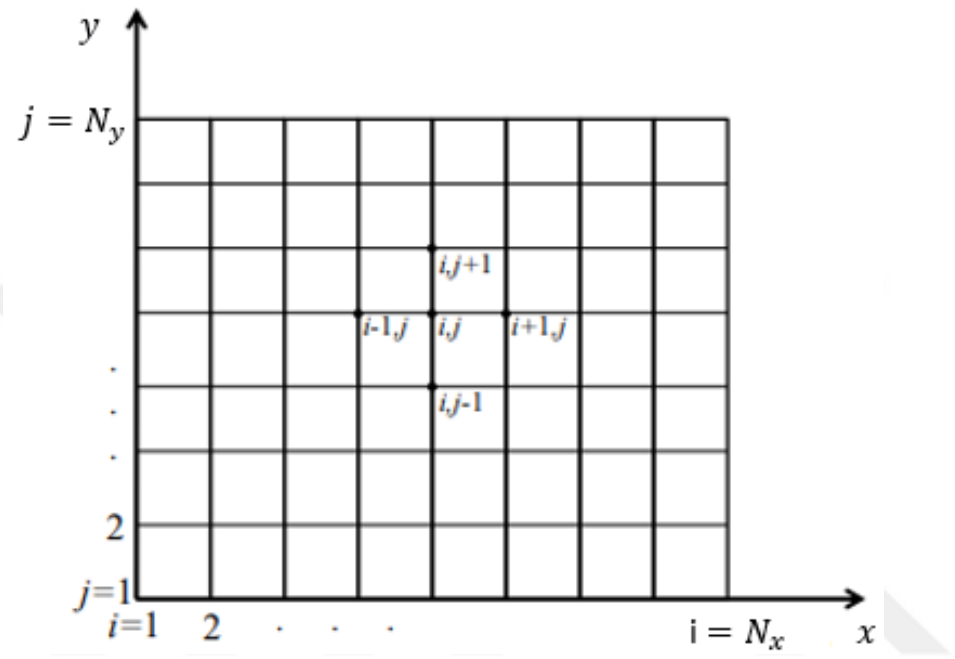

Figure 3.1. Discretization of mid-plane of a plate

Figure 3.1 shows the discretization of the mid-plane of the graded fiber-reinforced composite plate. The plate is divided by N_x grid points in x , and by N_y grid points in y directions, respectively. There is a total of N_xN_y nodes in the plate. The unknown displacements for the plate subjected to thermal load are u, v, and w. A linear set of equations need to be solved to find the minimum temperature that will buckle this plate. Therefore, it is necessary to know the derivatives of u, v, and w. Derivatives of $u(x,y), v(x,y)$,and $w(x,y)$ at points (i,j) with respect to x and y are found using DQM.

Derivatives of $u(x,y)$ with respect to x,y can be calculated below.

$$\frac{\partial u}{\partial x} = \sum_{k=1}^{N_x} A_{ik}^{(1)} u_{kj} \qquad \textbf{(3.8)}$$

$$\frac{\partial u}{\partial y} = \sum_{m=1}^{N_y} B_{jm}^{(1)} u_{im} \quad \textbf{(3.9)}$$

$$\frac{\partial^2 u}{\partial x^2} = \sum_{k=1}^{N_x} A_{ik}^{(2)} u_{kj} \quad \textbf{(3.10)}$$

$$\frac{\partial^2 u}{\partial y^2} = \sum_{m=1}^{N_y} B_{jm}^{(2)} u_{im} \quad \textbf{(3.11)}$$

$$\frac{\partial^3 u}{\partial x^2 \partial y} = \sum_{k=1}^{N_x} \sum_{m=1}^{N_y} A_{ik}^{(2)} B_{jm}^{(1)} u_{km} \quad \textbf{(3.12)}$$

$$\frac{\partial^3 u}{\partial x \partial y^2} = \sum_{k=1}^{N_x} \sum_{m=1}^{N_y} A_{ik}^{(1)} B_{jm}^{(2)} u_{km} \quad \textbf{(3.13)}$$

$$\frac{\partial^3 u}{\partial x^3} = \sum_{k=1}^{N_x} A_{ik}^{(3)} u_{kj} \quad \textbf{(3.14)}$$

$$\frac{\partial^3 u}{\partial y^3} = \sum_{m=1}^{N_y} B_{jm}^{(3)} u_{im} \quad \textbf{(3.15)}$$

$$\frac{\partial^4 u}{\partial x \partial y^3} = \sum_{k=1}^{N_x} \sum_{m=1}^{N_y} A_{ik}^{(1)} B_{jm}^{(3)} u_{km} \quad \textbf{(3.16)}$$

$$\frac{\partial^4 u}{\partial x^2 \partial y^2} = \sum_{k=1}^{N_x} \sum_{m=1}^{N_y} A_{ik}^{(2)} B_{jm}^{(2)} u_{km} \quad \textbf{(3.17)}$$

$$\frac{\partial^4 u}{\partial x^3 \partial y} = \sum_{k=1}^{N_x} \sum_{m=1}^{N_y} A_{ik}^{(3)} B_{jm}^{(1)} u_{km} \quad \textbf{(3.18)}$$

$$\frac{\partial^4 u}{\partial x^4} = \sum_{k=1}^{N_x} A_{ij}^{(4)} u_{kj} \quad \textbf{(3.19)}$$

$$\frac{\partial^4 u}{\partial y^4} = \sum_{m=1}^{N_y} B_{jm}^{(4)} u_{im} \quad \textbf{(3.20)}$$

Derivatives of $v(x,y)$ and $w(x,y)$ with respect to x and y are calculated like derivatives of $u(x,y)$. Derivatives calculated by DQM are substituted for derivatives in equations (2.80), (2.81), and (2.82). These equations are made more convenient. By applying DQM to the equations (2.80) – (2.82) the following equations can be reached.

$$\begin{aligned} & A_{11}\sum_{k=1}^{N_x} A_{ik}^{(2)}\,u_{kj} + 2A_{16}\sum_{k=1}^{N_x}\sum_{m=1}^{N_y} A_{ik}^{(1)}B_{jm}^{(1)}\,u_{km} + A_{66}\sum_{m=1}^{N_y} B_{jm}^{(2)}\,u_{im} \\ & \quad + A_{16}\sum_{k=1}^{N_x} A_{ik}^{(2)}\,v_{kj} + (A_{12}+A_{66})\sum_{k=1}^{N_x}\sum_{m=1}^{N_y} A_{ik}^{(1)}B_{jm}^{(1)}\,v_{km} \\ & \quad + A_{26}\sum_{m=1}^{N_y} B_{jm}^{(2)}\,v_{im} \\ & \quad - \Bigg(B_{11}\sum_{k=1}^{N_x} A_{ij}^{(3)}\,w_{kj} + 3B_{16}\sum_{k=1}^{N_x}\sum_{m=1}^{N_y} A_{ik}^{(2)}B_{jm}^{(1)}\,w_{km} \\ & \quad + (B_{12}+2B_{66})\sum_{k=1}^{N_x}\sum_{m=1}^{N_y} A_{ik}^{(1)}B_{jm}^{(2)}\,w_{km} + B_{26}\sum_{m=1}^{N_y} B_{jm}^{(3)}\,w_{im} \Bigg) \\ & \quad = 0 \end{aligned} \tag{3.21}$$

$$\begin{aligned} & A_{16}\sum_{k=1}^{N_x} A_{ik}^{(2)}\,u_{kj} + (A_{12}+A_{66})\sum_{k=1}^{N_x}\sum_{m=1}^{N_y} A_{ik}^{(1)}B_{jm}^{(1)}\,u_{km} + A_{26}\sum_{m=1}^{N_y} B_{jm}^{(2)}\,u_{im} \\ & \quad + A_{66}\sum_{k=1}^{N_x} A_{ik}^{(2)}\,v_{kj} + 2A_{26}\sum_{k=1}^{N_x}\sum_{m=1}^{N_y} A_{ik}^{(1)}B_{jm}^{(1)}\,v_{km} \\ & \quad + A_{22}\sum_{m=1}^{N_y} B_{jm}^{(2)}\,v_{im} \\ & \quad - \Bigg(B_{16}\sum_{k=1}^{N_x} A_{ik}^{(3)}\,w_{kj} + (B_{12}+2B_{66})\sum_{k=1}^{N_x}\sum_{m=1}^{N_y} A_{ik}^{(2)}B_{jm}^{(1)}\,w_{km} \\ & \quad + 3B_{26}\sum_{k=1}^{N_x}\sum_{m=1}^{N_y} A_{ik}^{(1)}B_{jm}^{(2)}\,w_{km} + B_{22}\sum_{m=1}^{N_y} B_{jm}^{(3)}\,w_{im} \Bigg) = 0 \end{aligned} \tag{3.22}$$

$$
\begin{aligned}
&B_{11}\sum_{k=1}^{N_x} A_{ik}^{(3)}\,u_{kj} + 3B_{16}\sum_{k=1}^{N_x}\sum_{m=1}^{N_y} A_{ik}^{(2)}B_{jm}^{(1)}\,u_{km} \\
&\quad + (B_{12}+2B_{66})\sum_{k=1}^{N_x}\sum_{m=1}^{N_y} A_{ik}^{(1)}B_{jm}^{(2)}\,u_{km} + B_{26}\sum_{m=1}^{N_y} B_{jm}^{(3)}\,u_{im} \\
&\quad + B_{16}\sum_{k=1}^{N_x} A_{ik}^{(3)}\,v_{kj} + (B_{12}+2B_{66})\sum_{k=1}^{N_x}\sum_{m=1}^{N_y} A_{ik}^{(2)}B_{jm}^{(1)}\,v_{km} \\
&\quad + 3B_{26}\sum_{k=1}^{N_x}\sum_{m=1}^{N_y} A_{ik}^{(1)}B_{jm}^{(2)}\,v_{km} + B_{22}\sum_{m=1}^{N_y} B_{jm}^{(3)}\,v_{im} \\
&\quad - \Bigg[D_{11}\sum_{k=1}^{N_x} A_{ik}^{(4)}\,w_{kj} + 2(D_{12}+2D_{66})\sum_{k=1}^{N_x}\sum_{m=1}^{N_y} A_{ik}^{(2)}B_{jm}^{(2)}\,w_{km} \\
&\quad + 4D_{16}\sum_{k=1}^{N_x}\sum_{m=1}^{N_y} A_{ik}^{(3)}B_{jm}^{(1)}\,w_{km} + 4D_{26}\sum_{k=1}^{N_x}\sum_{m=1}^{N_y} A_{ik}^{(1)}B_{jm}^{(3)}\,w_{km} \\
&\quad + D_{22}\sum_{m=1}^{N_y} B_{jm}^{(4)}\,w_{im} + \overline{N}_{xx}{}^{T}\sum_{k=1}^{N_x} A_{ik}^{(2)}\,w_{kj} + \overline{N}_{yy}{}^{T}\sum_{m=1}^{N_y} B_{jm}^{(2)}\,w_{im} \Bigg] \\
&\quad = 0
\end{aligned}
\tag{3.23}
$$

Simply supported boundary conditions can be written in DQM form as below.

$$x = 0, a\,; u_{ij} = v_{ij} = w_{ij} = 0\,; \tag{3.24}$$

$$
\begin{aligned}
M_{xx} = {} & B_{11}\sum_{k=1}^{N_x} A_{ik}^{(1)}\,u_{kj} + B_{12}\sum_{m=1}^{N_y} B_{jm}^{(1)}\,v_{im} + B_{16}\sum_{m=1}^{N_y} B_{jm}^{(1)}\,u_{im} \\
& + B_{16}\sum_{k=1}^{N_x} A_{ik}^{(1)}\,v_{kj} \\
& - \Bigg(D_{11}\sum_{k=1}^{N_x} A_{ik}^{(2)}\,w_{kj} + D_{12}\sum_{m=1}^{N_y} B_{jm}^{(2)}\,w_{im} \\
& + 2D_{16}\sum_{k=1}^{N_x}\sum_{m=1}^{N_y} A_{ik}^{(1)}B_{jm}^{(1)}\,w_{km} \Bigg) = 0
\end{aligned}
\tag{3.25}
$$

$$y = 0, b\,; u_{ij} = v_{ij} = w_{ij} = 0\,; \tag{3.26}$$

$$M_{yy} = B_{12}\sum_{k=1}^{N_x} A_{ik}^{(1)}\, u_{kj} + B_{22}\sum_{m=1}^{N_y} B_{jm}^{(1)}\, v_{im} + B_{26}\sum_{m=1}^{N_y} B_{jm}^{(1)}\, u_{im} + B_{26}\sum_{k=1}^{N_x} A_{ik}^{(1)}\, v_{kj} - \left(D_{12}\sum_{k=1}^{N_x} A_{ik}^{(2)}\, w_{kj} + D_{22}\sum_{m=1}^{N_y} B_{jm}^{(2)}\, w_{im} + 2D_{26}\sum_{k=1}^{N_x}\sum_{m=1}^{N_y} A_{ik}^{(1)} B_{jm}^{(1)}\, w_{km} \right) = 0 \quad \textbf{(3.27)}$$

Clamped boundary conditions can be represent in DQM form by the following algebraic expressions.

$$x = 0, a\,; u_{ij} = v_{ij} = w_{ij} = 0\,; \quad \textbf{(3.28)}$$

$$\frac{\partial w}{\partial x} = \sum_{k=1}^{N_x} A_{ik}^{(1)}\, w_{kj} = 0 \quad \textbf{(3.29)}$$

$$y = 0, b\,; u_{ij} = v_{ij} = w_{ij} = 0\,; \quad \textbf{(3.30)}$$

$$\frac{\partial w}{\partial y} = \sum_{m=1}^{N_y} B_{jm}^{(1)}\, w_{im} = 0 \quad \textbf{(3.31)}$$

The critical buckling temperature is obtained when the simply supported boundary condition and governing equations are solved together using the following steps.

$$\text{At } x = 0, a\,;\ u_{ij} = 0\ ; i = 1, N_x \quad \&\ j = 1,2, \ldots\ldots, N_y \quad \textbf{(3.32)}$$

$$\text{At } y = 0, b\,;\ u_{ij} = 0\ ; i = 2 \ldots\ldots, N_x - 1 \quad \&\ j = 1, N_y \quad \textbf{(3.33)}$$

By implementing boundary conditions for u at the boundary points lead to the linear equations as.

$$A_b d_b + A_d d_d = 0 \quad \textbf{(3.34)}$$

This algebraic expression consists of boundary equations written for u at each node in the boundary.

The displacements at the boundary nodes are expressed with d_b, and the displacements at the inner nodes are expressed with d_d. b represents boundary and d represents domain.

$$\{d_b\} = \{u_b, v_b, w_b\} \tag{3.35}$$

$$\{d_d\} = \{u_d, v_d, w_d\} \tag{3.36}$$

The matrices A_b and A_d are stiffness matrices associated with the boundary.

In boundary condition expressions written for each node at the boundary, the matrix formed by the displacement coefficients at the boundary is A_b, and the matrix formed by the displacement coefficients at the inner nodes is A_d.

Equation (3.21) for inner points is expressed below.

For $i = 2,3,\ldots..,N_x - 1 \quad \& \quad j = 2,3,\ldots.,N_y - 1$

$$\begin{aligned} & A_{11}\sum_{k=1}^{N_x} A_{ik}^{(2)}\, u_{kj} + 2A_{16}\sum_{k=1}^{N_x}\sum_{m=1}^{N_y} A_{ik}^{(1)} B_{jm}^{(1)}\, u_{km} + A_{66}\sum_{m=1}^{N_y} B_{jm}^{(2)}\, u_{im} \\ & \quad + A_{16}\sum_{k=1}^{N_x} A_{ik}^{(2)}\, v_{kj} + (A_{12} + A_{66})\sum_{k=1}^{N_x}\sum_{m=1}^{N_y} A_{ik}^{(1)} B_{jm}^{(1)}\, v_{km} \\ & \quad + A_{26}\sum_{m=1}^{N_y} B_{jm}^{(2)}\, v_{im} \\ & \quad - \left(B_{11}\sum_{k=1}^{N_x} A_{ik}^{(3)}\, w_{kj} + 3B_{16}\sum_{k=1}^{N_x}\sum_{m=1}^{N_y} A_{ik}^{(2)} B_{jm}^{(1)}\, w_{km} \right. \\ & \quad \left. + (B_{12} + 2B_{66})\sum_{k=1}^{N_x}\sum_{m=1}^{N_y} A_{ik}^{(1)} B_{jm}^{(2)}\, w_{km} + B_{26}\sum_{m=1}^{N_y} B_{jm}^{(3)}\, w_{im} \right) \\ & \quad = 0 \end{aligned} \tag{3.37}$$

Equation (3.37) can be written in a compact form like below.

$$A'_b d_b + A'_d d_d = 0 \tag{3.38}$$

In the governing equation written for each inner node, shown in (3.37), the stiffness matrix formed by the displacement coefficients in the boundary is shown with A'_b and the stiffness matrix formed by the displacement coefficients in the inner node is shown with A'_d.

When equation (3.34) and equation (3.38) are combined and written in matrix form, the following equations is obtained.

$$\begin{bmatrix} A_b & A_d \\ A'_b & A'_d \end{bmatrix} \begin{bmatrix} d_b \\ d_d \end{bmatrix} = [A][d] = 0 \tag{3.39}$$

$$[A] = \begin{bmatrix} A_b & A_d \\ A'_b & A'_d \end{bmatrix} \; ; \; [d] = \begin{bmatrix} d_b \\ d_d \end{bmatrix} \tag{3.40}$$

The boundary conditions for v are expressed as.

$$\text{At } x = 0, a \; ; \; v_{ij} = 0 \; ; i = 1, N_x \quad \& \; j = 1,2, \ldots\ldots, N_y \tag{3.41}$$

$$\text{At } y = 0, b \; ; \; v_{ij} = 0 \; ; i = 2 \ldots\ldots, N_x - 1 \quad \& \; j = 1, N_y \tag{3.42}$$

Boundary condition for v written in linear equation form is shown.

$$B_b d_b + B_d d_d = 0 \tag{3.43}$$

B_b is the stiffness matrix consisting of the coefficients of the displacement at the boundary and B_d is the stiffness matrix formed by the coefficients of the displacement at the inner node.

Equation (3.22) can be written in DQM form for inner nodes.

$$\text{For } i = 2,3, \ldots\ldots, N_x - 1 \quad \& \; j = 2,3, \ldots\ldots, N_y - 1$$

$$\begin{aligned} & A_{16} \sum_{k=1}^{N_x} A_{ik}^{(2)} u_{kj} + (A_{12} + A_{66}) \sum_{k=1}^{N_x} \sum_{m=1}^{N_y} A_{ik}^{(1)} B_{jm}^{(1)} u_{km} + A_{26} \sum_{m=1}^{N_y} B_{jm}^{(2)} u_{im} \\ & + A_{66} \sum_{k=1}^{N_x} A_{ik}^{(2)} v_{kj} + 2A_{26} \sum_{k=1}^{N_x} \sum_{m=1}^{N_y} A_{ik}^{(1)} B_{jm}^{(1)} v_{km} \\ & + A_{22} \sum_{m=1}^{N_y} B_{jm}^{(2)} v_{im} \\ & - \left(B_{16} \sum_{k=1}^{N_x} A_{ik}^{(3)} w_{kj} + (B_{12} + 2B_{66}) \sum_{k=1}^{N_x} \sum_{m=1}^{N_y} A_{ik}^{(2)} B_{jm}^{(1)} w_{km} \right. \\ & \left. + 3B_{26} \sum_{k=1}^{N_x} \sum_{m=1}^{N_y} A_{ik}^{(1)} B_{jm}^{(2)} w_{km} + B_{22} \sum_{m=1}^{N_y} B_{jm}^{(3)} w_{im} \right) = 0 \end{aligned} \tag{3.44}$$

This equation is written in linear equation form as follows.

$$B'_b d_b + B'_d d_d = 0 \tag{3.45}$$

$B'_b$and B'_d stiffness matrices seen in the equation written in linear form. They are the matrices formed by the displacement coefficients in the boundary and inner nodes, respectively. They can be obtained from the expressions coming from the equation (3.44) written in the DQM form.

When the two linear equations (3.43) and (3.45) are combined and made in matrix form, it looks like following.

$$\begin{bmatrix} B_b & B_d \\ B'_b & B'_d \end{bmatrix} \begin{bmatrix} d_b \\ d_d \end{bmatrix} = [B][d] = 0 \tag{3.46}$$

$$[B] = \begin{bmatrix} B_b & B_d \\ B'_b & B'_d \end{bmatrix} \tag{3.47}$$

The boundary condition expression for w, M_{xx} and M_{yy} is made in DQM form.

$$\text{At } x = 0, a\ ;\ w_{ij} = 0; M_{xx} = 0\ ; i = 1, N_x \quad \& \quad j = 1,2, \ldots\ldots, N_y \tag{3.48}$$

$$\text{At } y = 0, b\ ;\ w_{ij} = 0\ ; M_{yy} = 0\ ; i = 2,3\ \ldots., N_x - 1 \quad \& \quad j = 1, N_y \tag{3.49}$$

$$\begin{aligned} M_{xx} = B_{11} \sum_{k=1}^{N_x} A_{ik}^{(1)}\, u_{kj} + B_{12} \sum_{m=1}^{N_y} B_{jm}^{(1)}\, v_{im} + B_{16} \sum_{m=1}^{N_y} B_{jm}^{(1)}\, u_{im} \\ + B_{16} \sum_{k=1}^{N_x} A_{ik}^{(1)}\, v_{kj} \\ - \left(D_{11} \sum_{k=1}^{N_x} A_{ik}^{(2)}\, w_{kj} + D_{12} \sum_{m=1}^{N_y} B_{jm}^{(2)}\, w_{im} \right. \\ \left. + 2D_{16} \sum_{k=1}^{N_x} \sum_{m=1}^{N_y} A_{ik}^{(1)} B_{jm}^{(1)}\, w_{km} \right) = 0 \end{aligned} \tag{3.50}$$

$$M_{yy} = B_{12}\sum_{k=1}^{N_x} A_{ik}^{(1)}\, u_{kj} + B_{22}\sum_{m=1}^{N_y} B_{jm}^{(1)}\, v_{im} + B_{26}\sum_{m=1}^{N_y} B_{jm}^{(1)}\, u_{im} + B_{26}\sum_{k=1}^{N_x} A_{ik}^{(1)}\, v_{kj} - \left(D_{12}\sum_{k=1}^{N_x} A_{ik}^{(2)}\, w_{kj} + D_{22}\sum_{m=1}^{N_y} B_{jm}^{(2)}\, w_{im} + 2D_{26}\sum_{k=1}^{N_x}\sum_{m=1}^{N_y} A_{ik}^{(1)} B_{jm}^{(1)}\, w_{km} \right) = 0 \quad \textbf{(3.51)}$$

The boundary conditions written for the nodes in the boundary are expressed in the form of the linear equation as.

$$C_b d_b + C_d d_d = 0 \quad \textbf{(3.52)}$$

C_b and C_d are stiffness matrices related to the boundary conditions. C_b comes from coefficients of the displacements at the boundary points, and C_d comes from coefficients of displacements at inner points.

By implementing equation (3.23) for remaining inner nodes following equation is obtained in DQM form.

For $i = 3,4,\ldots..,N_x - 2$ & $j = 3,4,\ldots.,N_y - 2$

$$
\begin{aligned}
&B_{11}\sum_{k=1}^{N_x} A_{ik}^{(3)}\,u_{kj} + 3B_{16}\sum_{k=1}^{N_x}\sum_{m=1}^{N_y} A_{ik}^{(2)}B_{jm}^{(1)}\,u_{km} \\
&\quad + (B_{12}+2B_{66})\sum_{k=1}^{N_x}\sum_{m=1}^{N_y} A_{ik}^{(1)}B_{jm}^{(2)}\,u_{km} + B_{26}\sum_{m=1}^{N_y} B_{jm}^{(3)}\,u_{im} \\
&\quad + B_{16}\sum_{k=1}^{N_x} A_{ik}^{(3)}\,v_{kj} + (B_{12}+2B_{66})\sum_{k=1}^{N_x}\sum_{m=1}^{N_y} A_{ik}^{(2)}B_{jm}^{(1)}\,v_{km} \\
&\quad + 3B_{26}\sum_{k=1}^{N_x}\sum_{m=1}^{N_y} A_{ik}^{(1)}B_{jm}^{(2)}\,v_{km} + B_{22}\sum_{m=1}^{N_y} B_{jm}^{(3)}\,v_{im} \\
&\quad - \Bigg[D_{11}\sum_{k=1}^{N_x} A_{ik}^{(4)}\,w_{kj} + 2(D_{12}+2D_{66})\sum_{k=1}^{N_x}\sum_{m=1}^{N_y} A_{ik}^{(2)}B_{jm}^{(2)}\,w_{km} \\
&\quad + 4D_{16}\sum_{k=1}^{N_x}\sum_{m=1}^{N_y} A_{ik}^{(3)}B_{jm}^{(1)}\,w_{km} + 4D_{26}\sum_{k=1}^{N_x}\sum_{m=1}^{N_y} A_{ik}^{(1)}B_{jm}^{(3)}\,w_{km} \\
&\quad + D_{22}\sum_{m=1}^{N_y} B_{jm}^{(4)}\,w_{im} + \overline{N}_{xx}{}^{T}\sum_{k=1}^{N_x} A_{ik}^{(2)}\,w_{kj} + \overline{N}_{yy}{}^{T}\sum_{m=1}^{N_y} B_{jm}^{(2)}\,w_{im} \Bigg] \\
&\quad = 0
\end{aligned}
\tag{3.53}
$$

The above equation is expressed in compact form like below.

$$
C'_b d_b + C'_d d_d = \Delta T(F_b d_b + F_d d_d) \tag{3.54}
$$

C'_b is the stiffness matrix created by the displacement coefficients at the boundary points, and C'_d is the stiffness matrix formed by the displacement coefficients at the inner points.

F_b and F_d are the matrices consisting of the numerical values of the terms containing the temperature difference which are coming from the coefficients of the displacements at the boundary and the inner nodes, respectively.

When the equation (3.52) and equation (3.54) are assembled, the expression written below as matrix is reached.

$$
\begin{bmatrix} C_b & C_d \\ C'_b & C'_d \end{bmatrix}\begin{bmatrix} d_b \\ d_d \end{bmatrix} = [C][d] = \Delta T \begin{bmatrix} 0 & 0 \\ F_b & F_d \end{bmatrix}\begin{bmatrix} d_b \\ d_d \end{bmatrix} \tag{3.55}
$$

$$
[C] = \begin{bmatrix} C_b & C_d \\ C'_b & C'_d \end{bmatrix} \tag{3.56}
$$

By combining equation (3.39), equation (3.46), and equation (3.55) the following system of equation is obtained.

$$\begin{bmatrix}[A]\\[B]\\[C]\end{bmatrix}\begin{bmatrix}d_b\\d_d\end{bmatrix}=\Delta T\begin{bmatrix}[0] & [0]\\[0] & [0]\\[F_b] & [F_d]\end{bmatrix}\begin{bmatrix}d_b\\d_d\end{bmatrix} \tag{3.57}$$

$$\left\{\begin{bmatrix}[A]\\[B]\\[C]\end{bmatrix}-\Delta T\begin{bmatrix}[0] & [0]\\[0] & [0]\\[F_b] & [F_d]\end{bmatrix}\right\}\begin{bmatrix}d_b\\d_d\end{bmatrix}=0 \tag{3.58}$$

By using the eig command in MATLAB the eigenvalue solution is made for the equation in (3.58) and its critical buckling temperature can be found.

The solution procedure for the clamped boundary condition is the same as simply-supported. Only the equation $\frac{\partial w}{\partial x}=0$ instead of $M_{xx}=0$, and $\frac{\partial w}{\partial y}=0$ should be written instead of $M_{yy}=0$ at the required boundary points.

3.3 Finite Element Method

Finite element modeling was done using Abaqus. A two-dimensional plate was drawn using the sketch under the part tab. Then, the mechanical properties of the material constituting the ply were defined for each ply in the material part. In the next step, the section was created. Continuum shell composite was selected as the section type. In the section, the plies that make up the laminate is defined, and the material properties, thickness, and ply angles for the plies are entered. This section was assigned to the plate created in part. Finite element mesh was applied over the existing geometry. The element type used is S4R, and the mesh density is NxN. There are total of NxN nodes in the model. The S4R element used is shown in Figure 3.2. The S4R element consists of four nodes and one integration point. The meshed state of the plate is shown in Figure 3.3. Under the assembly tab, the assembly was created in the instances section. To find the desired failure mode, the procedure type linear perturbation was selected in the step section, and then the buckle option was selected. The boundary condition was given to the examined plate.

Under the BC tab, the pinned option for the simply supported boundary condition, and the encastre option for the clamped boundary condition was selected. Then, unit temperature difference was given to the examined plate in the predefined field part. The temperature difference given is constant through the region. All the parameters necessary to examine the problem are defined, and the model is prepared. The job was created to find the critical buckling temperature. Full analysis was selected as the job type, and it was ready to run. The created job was submitted for analysis. After the calculations were completed, the results were obtained in the result section. The eigenvalue value obtained is the critical buckling temperature value.

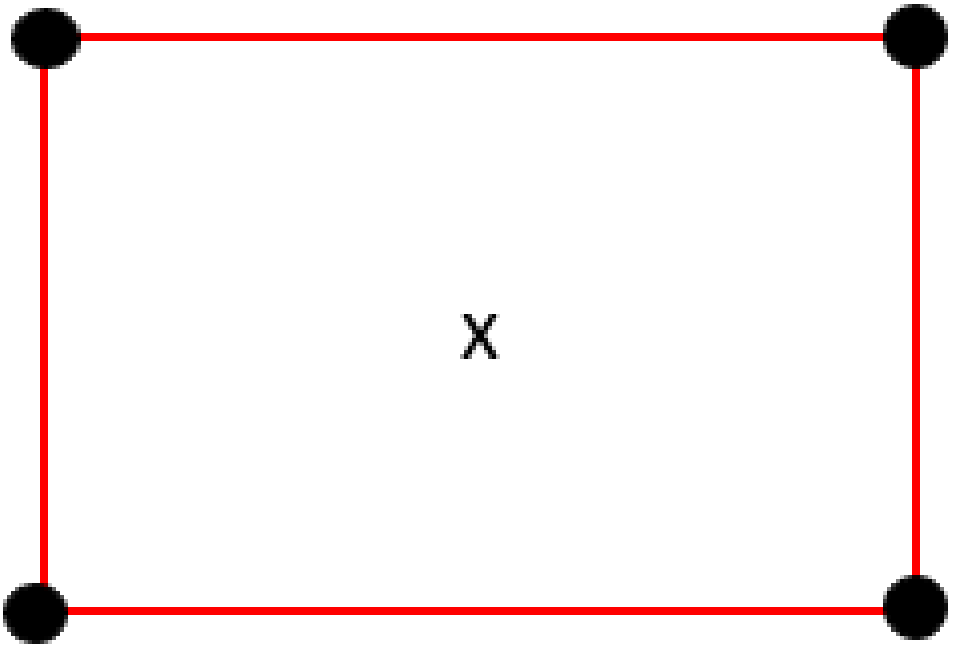

Figure 3.2. Figure of S4R element

S stands for shell, 4 shows number of nodes, and R stands for reduced integration.

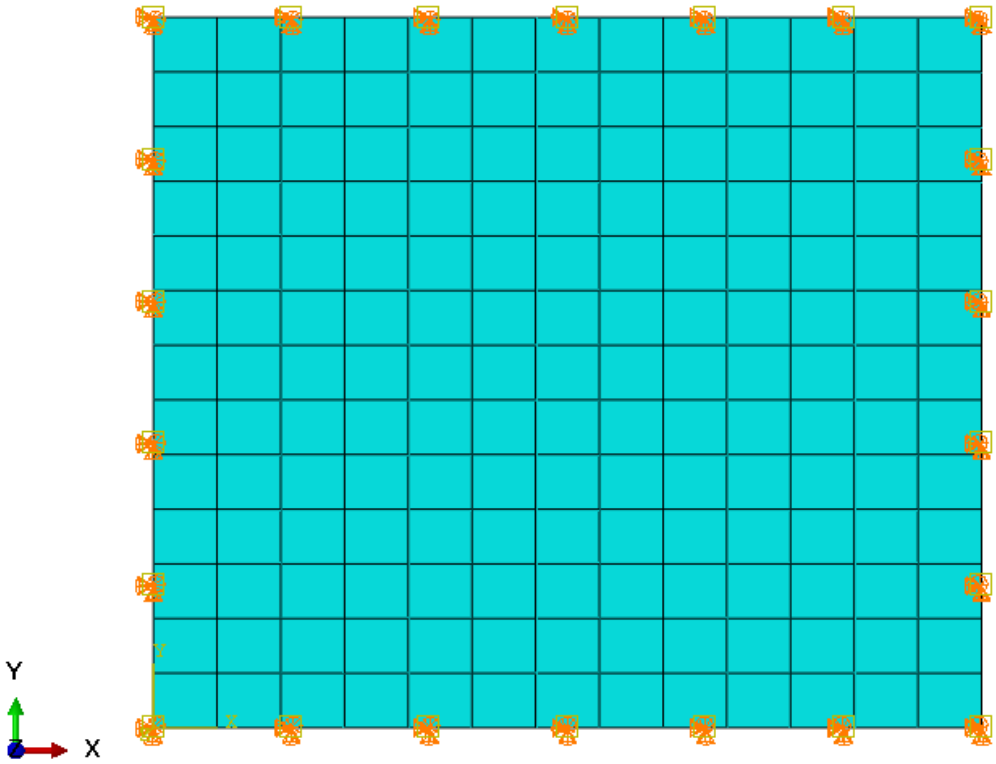

Figure 3.3. Finite element model

CHAPTER 4

NUMERICAL RESULT

The critical buckling temperature was calculated using the method mentioned in Chapter 3 for the graded fiber reinforcement composite plate. The minimum temperature difference that causes buckling is calculated for all edges of the plate simply supported (SSSS) or all edges clamped (CCCC).

4.1 Graded Fiber – Reinforced Material

Graded fiber-reinforced composite plate is composed of plies. Figure 2.3 shows a typical laminated composite plate. There are fiber and matrix in different volume fractions in each ply. The amount of fiber volume changes in the direction of thickness; thus, the material properties change. In Figure 4.1, the variation of fiber volume fraction along the thickness is seen. The material properties vary depending on the fiber volume fraction, and the effective material properties are obtained according to the micromechanical model [1].

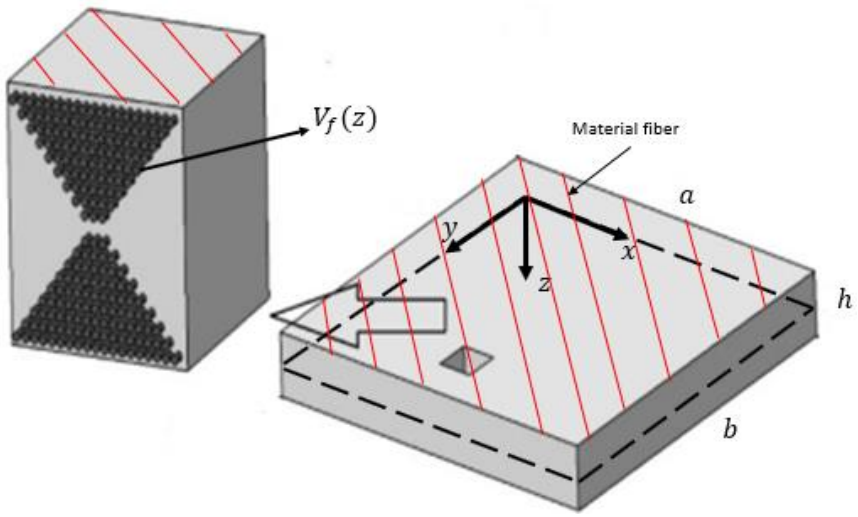

Figure 4.1. Laminated composite plate with variable fiber volume fraction

$$V_f(z) + V_m(z) = 1 \tag{4.1}$$

$$E_{11}(z) = E^f V_f(z) + E^m V_m(z) \tag{4.2}$$

$$\frac{1}{E_{22}(z)} = \frac{V_f(z)}{E^f} + \frac{V_m(z)}{E^m} - V_f(z)V_m(z)\frac{\frac{\upsilon^2{}_f E^m}{E^f} + \frac{\upsilon^2{}_m E^f}{E^m} - 2\upsilon^f \upsilon^m}{V_f(z)E^f + V_m(z)E^m} \tag{4.3}$$

$$G_{12}(z) = \frac{G^f G^m}{G^f V_m(z) + G^m V_f(z)} \tag{4.4}$$

$$\upsilon_{12}(z) = V_f(z)\upsilon^f + V_m(z)\upsilon^m \tag{4.5}$$

$$\alpha_1(z) = \frac{V_f(z)E^f\alpha^f + V_m(z)E^m\alpha^m}{V_f(z)E^f + V_m(z)E^m} \tag{4.6}$$

$$\alpha_2(z) = (1+\upsilon^f)V_f(z)\alpha^f + (1+\upsilon^m)V_m(z)\alpha^m - \upsilon_{12}(z)\alpha_1(z) \tag{4.7}$$

V_f , E^f , G^f, and υ^f are the volume fraction, young's modulus, shear modulus and poisson's ratio of the fiber. V_m, E^m, G^m and υ^m are the corresponding properties for the matrix.

where α^f, and α^m are called the thermal expansion coefficients of the fiber and matrix.

The terms E_{11}, E_{22}, and G_{12} are longitudinal , transverse and in plane shear modulus, respectively.Longitudinal and transverse directions of the fiber-reinforced composite plate are shown in Figure 2.4.

υ_{12}, α_1, and α_2 are poisson ratio , longitudinal thermal expansion coefficient and transverse thermal expansion coefficient.

4.2 Verification

To check the accuracy of the study, it is necessary to make comparisons to the results given in previously published articles. With close results, it can be inferred that the method developed leads to accurate results. Waily [24] carried out thermal buckling analysis for simply - supported rectangular plates. The plate's temperature, which initially had a constant uniform temperature, was increased uniformly. Due to the temperature difference, reaction forces formed in the boundary. Figure 4.2 shows the compressive axial forces formed at the boundary. The plate began to buckle with the effect of these compressive reaction forces. Waily [24] calculated the critical temperature, which creates the force that will buckle the plate in this study. The dimensions of the rectangular plate examined in the study are a, b, and h. a length, b width, and h represent thickness. The length and width of the plate are 200 mm, and its thickness is 5 mm. The plate is a unidirectional composite plate consisting of fiber and matrix. Glass-E-fibers were used as the fiber, and polyester resin was used as the matrix. To observe the effect of the matrix type on the critical buckling temperature, the critical buckling temperatures of the plate consisting of Glass-E-fibers and polyester resin and the plate consisting of Glass-E-fibers and epoxy resin were calculated. The mechanical properties of the material used in these calculations are given below.

Glass -E-Fibers

$E^f = 74\ (GPa)$, $G^f = 30\ (GPa)$, $\upsilon^f = 0.25$, $\alpha^f = 0.5 * 10^{-5}\ (°C^{-1})$

Polyester Resin

$E^m = 4\ (GPa)$, $G^m = 1.4\ (GPa)$, $\upsilon^m = 0.4$, $\alpha^m = 8 * 10^{-5}\ (°C^{-1})$

Epoxy Resin

$E^m = 4.5\ (GPa)$, $G^m = 1.6\ (GPa)$, $\upsilon^m = 0.4$, $\alpha^m = 11 * 10^{-5}\ (°C^{-1})$

In Table 4.1, the critical buckling temperature was calculated for the composite plate consisting of unidirectional Glass-E-fibers and polyester resin. Convergence study was carried out for 0.1 fiber volume fraction.

Table 4.1 Convergence study on critical buckling temperature of SSSS unidirectional fiber-reinforced composite plate $a = 200\ mm$, $\frac{a}{b} = 1$, $h = 5\ mm$, $V_f = 0.1$

NxN	**DQM** (℃)	**[24]** (℃)
9x9	13.6739	13.6752
11x11	13.6748	13.6752
13x13	13.6752	13.6752
15x15	13.6752	13.6752
17x17	13.6752	13.6752

Table 4.1 shows the critical buckling temperature value according to the number of grid points in the x and y directions used in DQM. Considering the convergence of the results, $N = 13$ should be used to obtain more accurate results.

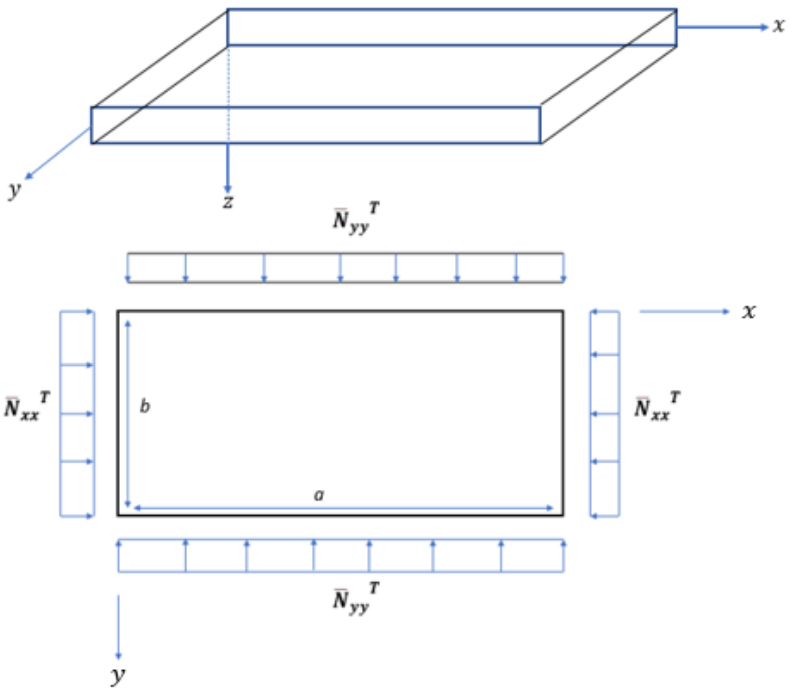

Figure 4.2. In-plane axial compressive force due to thermal effects

Thermal buckling result of the unidirectional fiber-reinforced composite plate are shown in Figure 4.3. In Figure 4.3, the minimum buckling temperature that will buckle the composite plates are found for each fiber volume fraction. In Figure 4.4, the effect of the resins on the structure's critical buckling temperature is observed using different resins. In Figure 4.5, the critical buckling temperature of the composite plate is obtained for three different fiber volume fractions according to the aspect ratio. The buckling results for the fiber-reinforced composite plate are provided in Figures 4.3 - 4.5. According to the results, if the amount of fiber volume fraction in the composite plate increases, the critical temperature value that will buckle the structure increases. It is seen that the resins affect the thermal strength of the structure. Finally, if the dimensions of the plate increase, the minimum temperature value that will buckle the structure decreases. As seen in Figure 4.4 ,the effect of fiber volume fraction on critical buckling temperature is linear, while in Figure 4.5, aspect ratio effect on critical buckling temperature is exponential. Therefore, the change in aspect ratio affects the critical buckling temperature more than the change in fiber volume fraction. The results obtained are in excellent agreement with the studies of Waily [24].

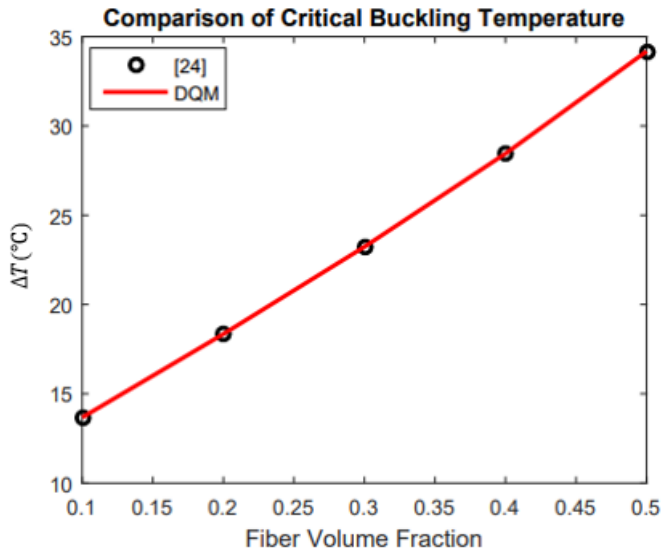

Figure 4.3. Critical buckling temperature of SSSS unidirectional composite plate with glass fiber and polyester resin, $a = 200\ mm$,$\frac{a}{b} = 1$,$h = 5\ mm$

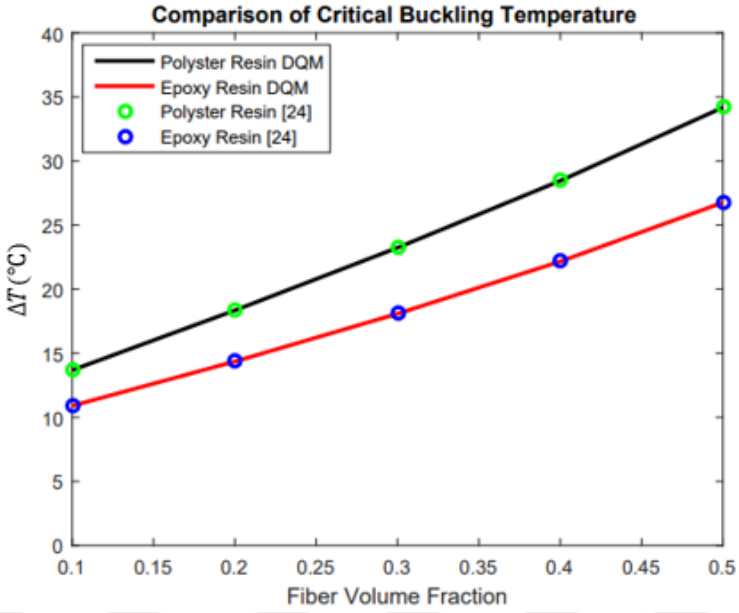

Figure 4.4. Critical buckling temperature of SSSS unidirectional composite plate with glass fiber and different resin, $a = 200\ mm$,$\frac{a}{b} = 1$,$h = 5\ mm$

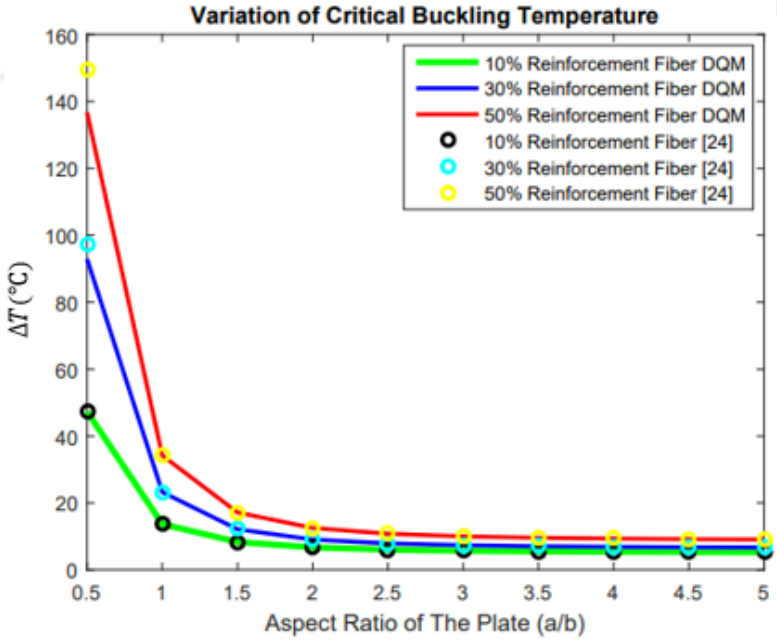

Figure 4.5. Critical buckling temperature of SSSS unidirectional composite plate with different aspect ratio for different fiber volume fraction of glass fiber and polyester resin, $b = 200\ mm$,$h = 5\ mm$

4.3 Finite Element Analysis

In this part, the critical buckling temperature value of the composite plate was calculated by finite element analysis. To test the accuracy of the finite element model, the problem in [24] was modeled with Abaqus, and the critical buckling temperature value was calculated. The mesh density in the model is 13x13, and the element type used is S4R. In DQM, the plate is divided into 13 grid points in the x direction and 13 in the y direction. The critical buckling temperature value calculated with Abaqus, and the critical buckling temperature value calculated using DQM are compared. The dimensions of the examined plate are $200x200$ mm, and its thickness is $5\ mm$. The plate is a unidirectional composite plate consisting of Glass-E-fiber and polyester resin. The temperature of the simply- supported plate, which has a uniform initial temperature, was increased uniformly. After a certain temperature difference, the plate started to buckle. The minimum temperature that creates this condition is called the critical buckling temperature. The critical buckling temperature value for five different fiber volume fractions was calculated using FEA and DQM.

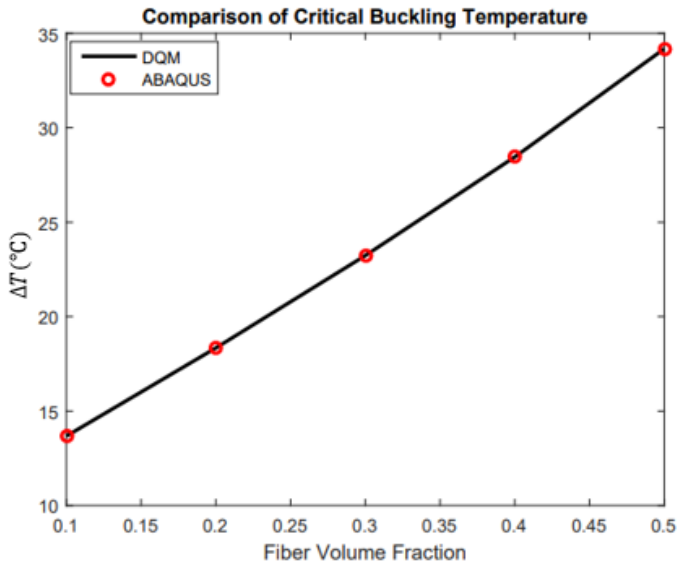

Figure 4.6. Critical buckling temperature of SSSS unidirectional composite plate with glass fiber and polyester resin, $a = 200\ mm$,$\frac{a}{b} = 1$,$h = 5\ mm$

In Figure 4.6, the critical buckling temperature of the unidirectional non-graded fiber reinforcement composite plate was calculated with the help of Abaqus. The results of the Abaqus model were compared with the study examined in the literature, and the same results were obtained with the results in the literature. In this way, the Abaqus model is correlated. As the Abaqus model has been validated, the results in these studies will be compared with the Abaqus model.

One more validation was done for FEA and DQM. This time, calculations were made for the plate with dimensions of $200x200$ mm and a thickness of 4 mm. This plate also consists of Glass-E-fiber and polyester resin. Unlike the previous one, this plate is not unidirectional. It is a symmetrical plate composed of 8 plies. The thickness of each ply is 0.5 mm, and the laying angles are $[60/45/-45/30]_s$. The mesh density used in FEA is $13x13$, and the element type is S4R. In DQM, the plate is divided into 13 grid points in the x direction and 13 in the y direction. The plate is simply-supported and has an initial uniform temperature. The plate's temperature was increased uniformly, and the critical buckling temperature value that would buckle the plate was calculated by both FEA and DQM.

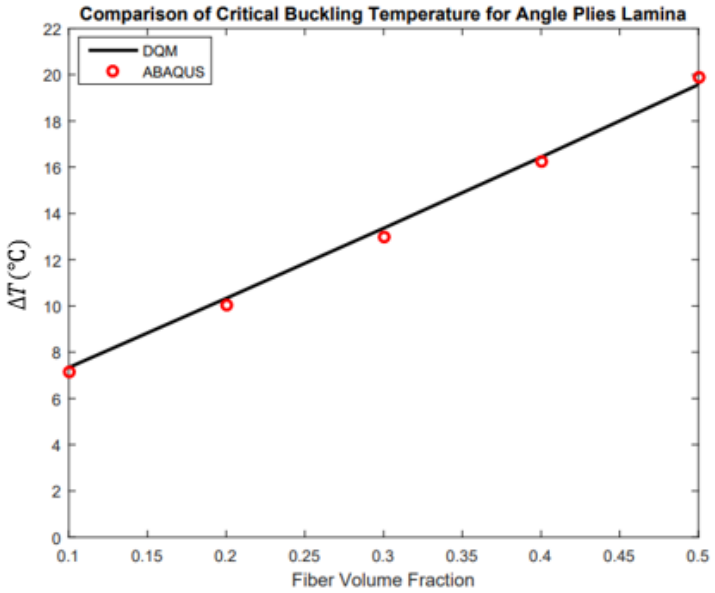

Figure 4.7. Critical buckling temperature of SSSS $[60/45/-45\ /30]_s$ angle plies composite plate with glass fiber and epoxy resin, $a = 200\ mm$,$\frac{a}{b} = 1$,$h = 4\ mm$

In Figure 4.7, the critical buckling temperature of the symmetrical composite plate formed by the plies with different laying angles was calculated. As the fiber volume fraction in the plate increases, the critical temperature value that will buckle the structure increases. There is excellent agreement between the results obtained in this study and those in Abaqus.

4.4 Numerical Results for Symmetric Laminates

Critical buckling temperature was calculated for a $200x200$ mm symmetrically laminated composite plate with varying fiber volume fractions. The plate contains eight plies with $[60/-30/90/45]_s$ laying angles and is simply supported from the edges. The plies are composed of Glass-E-fiber and polyester resin. The composite plate is graded in the thickness direction. Gradation is provided by the fiber volume fraction changing in the z-direction. The fiber volume function is $V_f(z) = 0.4(\frac{|z|}{h})$. Table 4.2 shows the laying angles and fiber volume fraction of the plies. The plate has an initial uniform temperature, which is then uniformly increased. After a while, it started to buckle under the axial compressive force caused by the boundary conditions at a certain temperature difference. The critical buckling temperature value that caused this load was calculated using FEA and DQM for five different plate thicknesses. The mesh density used is $13x13$, and the element type is S4R.In DQM, the plate is divided into 13 grid points, each in the x and y directions.

Table 4.2 Plate's lamination scheme and fiber volume fraction of each ply

Plies	V_f	**Orientation Angle (°)**
Ply 1	0.4	60
Ply 2	0.3	-30
Ply 3	0.2	90
Ply 4	0.1	45
Ply 5	0.1	45
Ply 6	0.2	90
Ply 7	0.3	-30
Ply 8	0.4	60

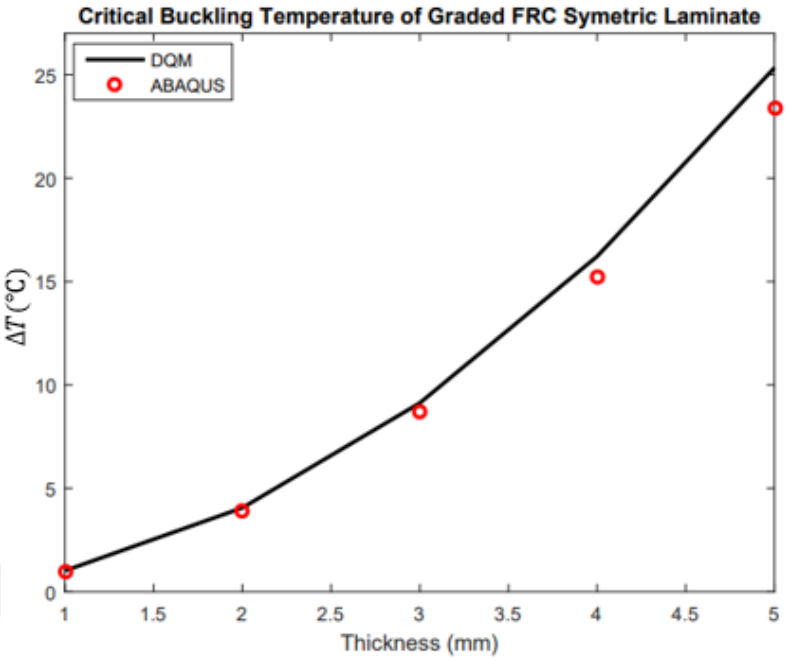

Figure 4.8. Critical buckling temperature of SSSS $[60/-30/90/45]_s$ angle plies composite plate with glass fiber and epoxy resin, $a = 200\,mm$,$\frac{a}{b} = 1$,$V_f(z) = 0.4(\frac{|z|}{h})$

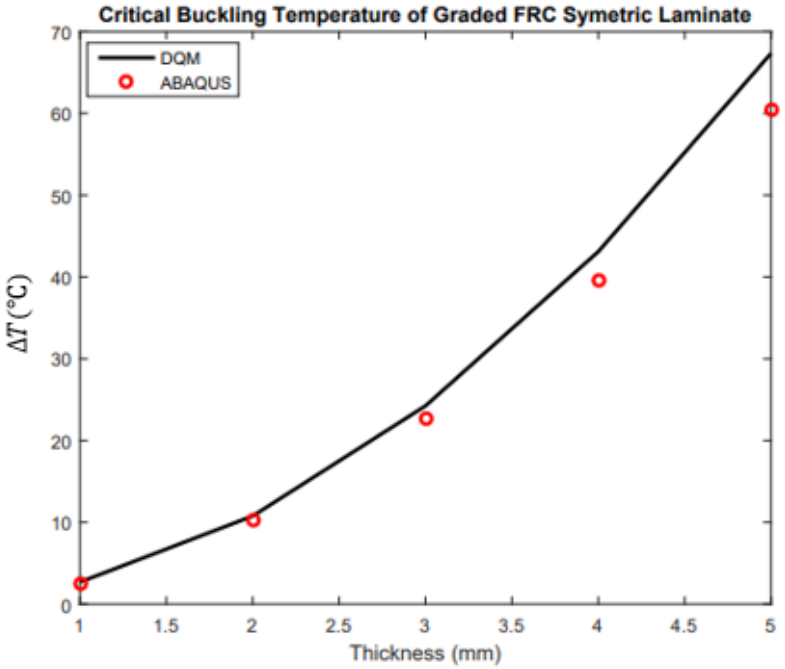

Figure 4.9. Critical buckling temperature of SSSS $[60/-30/90/45]_s$ angle plies composite plate with glass fiber and epoxy resin, $a = 200\,mm$,$\frac{a}{b} = 2$,$V_f(z) = 0.4(\frac{|z|}{h})$

In Figure 4.8, the critical buckling temperature was calculated for the graded fiber reinforcement composite plate. The examined composite plate is symmetrical according to the laying angle. As the thickness of the plate increases, the critical buckling temperature increases. There is a good agreement between the results obtained in this study and the results in Abaqus. However, after a certain thickness value, there is some variation between the results. Since the theory used in this study is valid for thin plates, the plate becomes thicker as the thickness increases, and therefore, the results deviate a little when the thickness increases. In Figure 4.9, the critical buckling temperature of the structure was calculated for one dimension of the graded fiber reinforcement composite plate halved. As in the previous graph, after a certain thickness, there was some deviation between the results obtained in the study and those in Abaqus. When the critical temperatures in the two figures are compared, the critical temperature value that will buckle the plate increases significantly when the plate dimensions are reduced. As the panel dimension from the loading direction increases, the resistance of the panel against deformation decreases. Therefore, the increasing aspect ratio with the increase in the size of panel causes a decrease in the stiffness value of the panel. Critical buckling temperature value decreases depending on the increase in the aspect ratio.

The effect of some parameters on the buckling behavior of the laminated composite plate was investigated. The change in the critical buckling temperature of the plate was investigated by changing the a/b ratio for the plate shown in Figure 4.1. The plate is simply- supported from the edges. The b value for the examined plate is 100 mm, the h is 1 mm, and a value change. This composite plate contains eight plies consisting of Glass-E-fiber and polyester resin. The fiber volume fraction and ply orientation of the plies are as in Table 4.2.

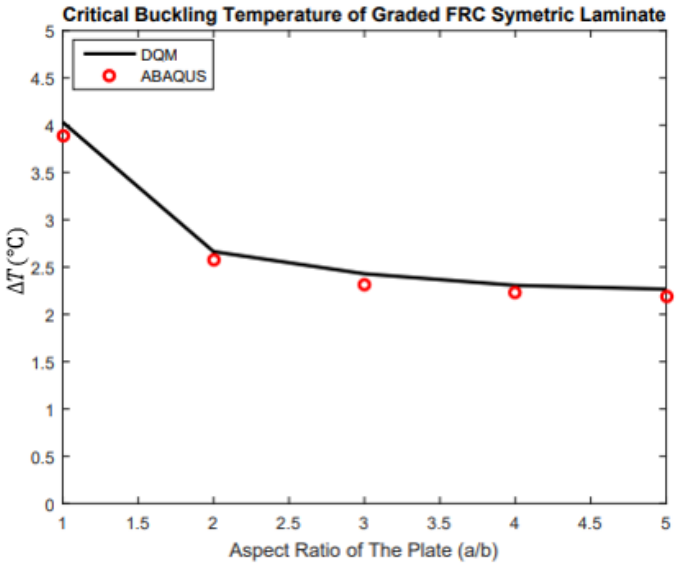

Figure 4.10. Critical buckling temperature of SSSS $[60/-30/90/45]_s$ angle plies composite plate with glass fiber and epoxy resin, $b = 100\ mm$,$h = 1.0\ mm$

$$V_f(z) = 0.4(\frac{|z|}{h})$$

In Figure 4.11, the critical buckling temperature value was calculated by changing the b/a ratio for the plate expressed in Figure 4.1. In this case, a value is 100 mm, and the b value changes. All parameters except these are the same as in the previous example.

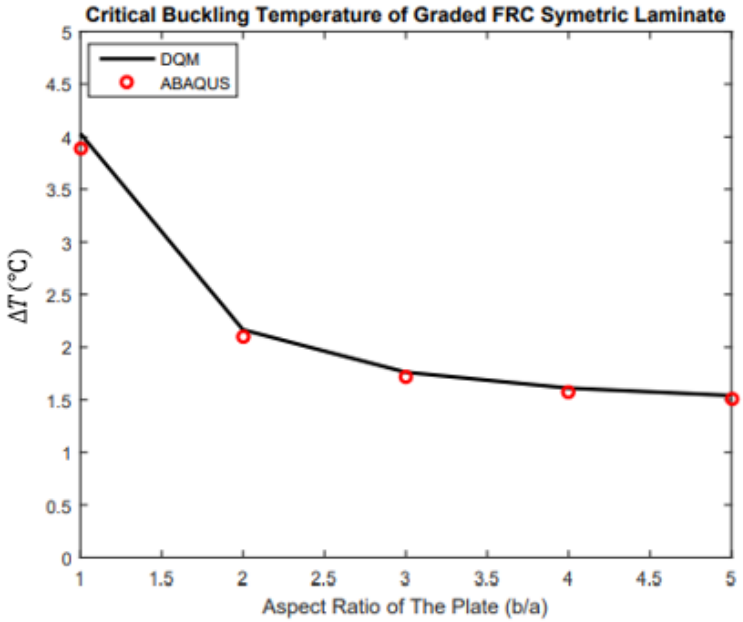

Figure 4.11. Critical buckling temperature of SSSS $[60/-30/90/45]_s$ angle plies composite plate with glass fiber and epoxy resin, $a = 100\ mm$,$h = 1.0\ mm$

$$V_f(z) = 0.4(\frac{|z|}{h})$$

In Figure 4.10, the critical buckling temperature value was calculated for the graded fiber reinforcement composite plate according to different aspect ratios. As can be seen from the results in the graph, as the dimensions of the plate increase, the critical temperature value required for the structure to undergo buckling decreases. In Figure 4.11, as in the previous graph, the effect of aspect ratio on critical buckling temperature is examined. Similar behavior is also seen here. When the dimensions of the panel increase, its resistance to the applied load decreases and it becomes easier for the panel to switch to the bending mode. When Figure 4.10 and Figure 4.11 are examined, the critical buckling temperature value of the panel decreases due to the increase in aspect ratio.

The effect of ply laying angles on critical buckling temperature was investigated. The a and b values for the plate shown in Figure 4.1 are 200 mm, and the plate is simply-supported from all edges. The composite plate consists of eight plies with same thickness value, and there are three different combinations according to the ply

laying angles. The stacking sequences are shown in Table 4.3. The material of the plies is as in the previous example. Critical buckling temperature was calculated at five different plate thickness values for three different stacking sequences. There is a good agreement between DQM-[24] and DQM-ABAQUS in the comparisons made so far. It is enough to calculate critical buckling temperature with DQM. Therefore, the effect of lamination scheme change on the critical buckling temperature has been investigated only with DQM. The plates is divided in 13 grid points in each x and y directions. The results from DQM is shown in Figure 4.12.

Table 4.3 Stacking sequences

Lamination Scheme Name	**Stacking Sequence**
Orientation 1	$[60/-30/90/45]_s$
Orientation 2	$[45/75/60/30]_s$
Orientation 3	$[90/75/60/0]_s$

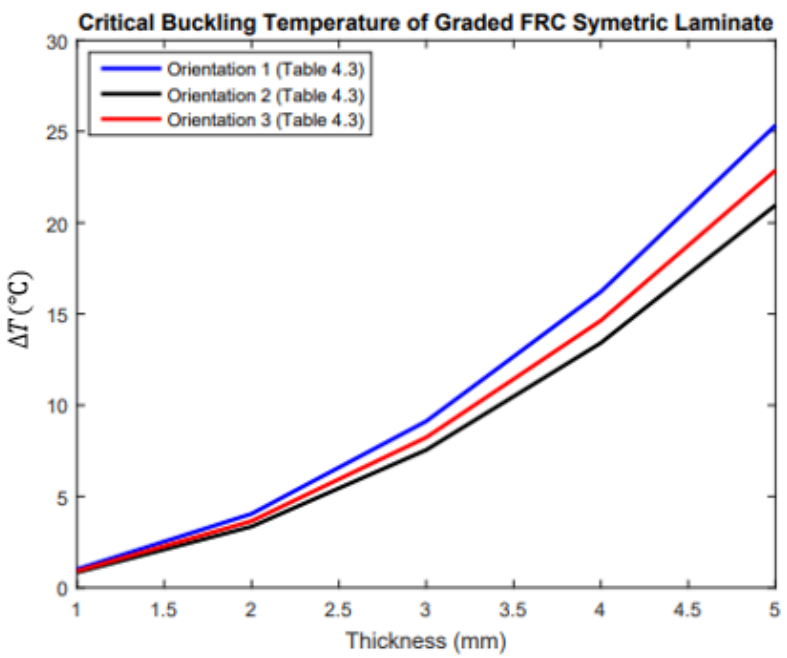

Figure 4.12. Critical buckling temperature of SSSS angle plies composite plate with glass fiber and epoxy resin from DQM, $a = 200\,mm$, $\frac{a}{b} = 1.0$, $V_f(z) = 0.4(\frac{|z|}{h})$

The effect of fiber orientation angle on the buckling behavior of the structure was investigated. The critical buckling temperature of the composite plate with symmetric ply sequence was found for three fiber angle configurations at different thicknesses. The temperature values are different for each orientation. It is understood from the results obtained that the fiber orientation angle affects the mechanical properties of the structure. When the composite structure is subjected to a load in the longitudinal direction $0°$,$30°$,$45°$,$60°$,and $90°$ angled plies carry the highest load respectively. For example, if the number of plies with $0°$ orientation increases, the amount of longitudinal load on plies decreases. Less load on the plies means more difficult buckling of structure. In the same manner, in the transverse direction increasing the number of $90°$ plies causes the structure to buckle more difficult. The number of certain angled plies changes the buckling characteristic of the structure according to the load direction. Depending on the applied load orientation, the distance between the orientation of the ply that carries the highest load and the plane where the plies first start to line up creates an extra bending moment. Due to the extra bending moment ,structure can buckle easily. Therefore, stacking sequence changes the buckle state of the structure.

The first four dominant mode shapes were found by using DQM and ABAQUS for the composite plate in Figure 4.1. For the plate in Figure 4.1, $a = 200$ mm, $b = 200$ mm, and $h = 1$ mm, the plate is simply-supported from all edges. The plate contains plies made of Glass-E-fiber and polyester resin. The plate consists of eight plies with equal thickness, and the fiber volume fraction and laying angles of each ply are shown in Table 4.2. Mode shapes obtained from DQM are shown in Figure 4.13, and mode shapes obtained from ABAQUS are shown in Figure 4.14.It is seen that the buckling mode shapes obtained for the same configurations in DQM, and ABAQUS are the same.

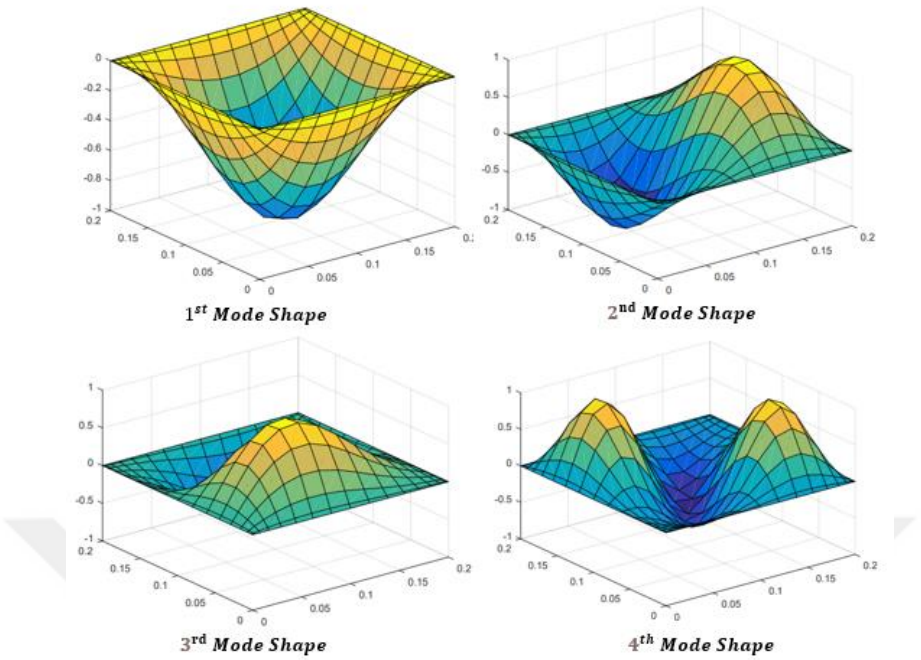

Figure 4.13. Dominant mode shapes of SSSS $[60/-30/90/45]_s$ angle plies composite plate with glass fiber and epoxy resin from DQM, $a = 200\,mm$, $\frac{a}{b} = 1.0$, $h = 1\,mm$, $V_f(z) = 0.4(\frac{|z|}{h})$

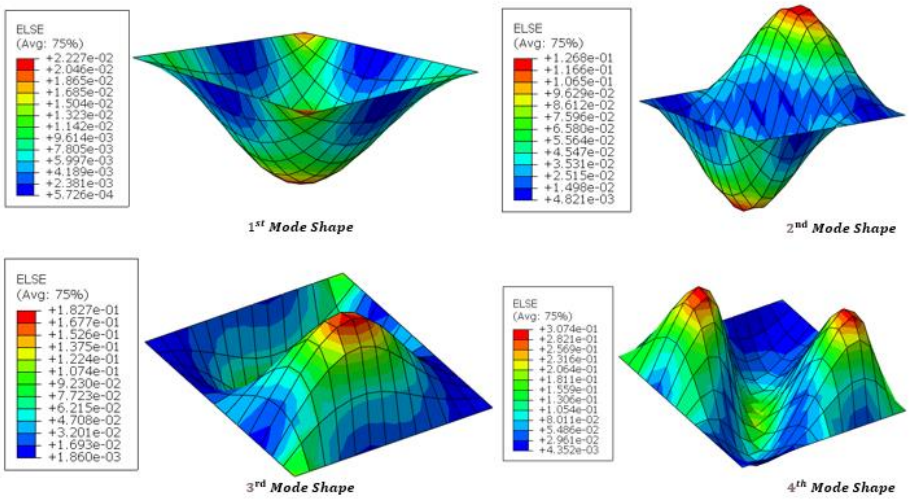

Figure 4.14. Dominant mode shapes of SSSS $[60/-30/90/45]_s$ angle plies composite plate with glass fiber and epoxy resin from ABAQUS , $a = 200\,mm$, $\frac{a}{b} = 1.0$, $h = 1\,mm$, $V_f(z) = 0.4(\frac{|z|}{h})$

In Figure 4.8, the boundary condition for the calculated state of the critical buckling temperature has been changed to clamped. Everything except the boundary condition has remained the same for the state, whose results are shown in Figure 4.8. The critical buckling temperature value calculated for five different thicknesses in the clamped boundary condition is shown in Figure 4.15.

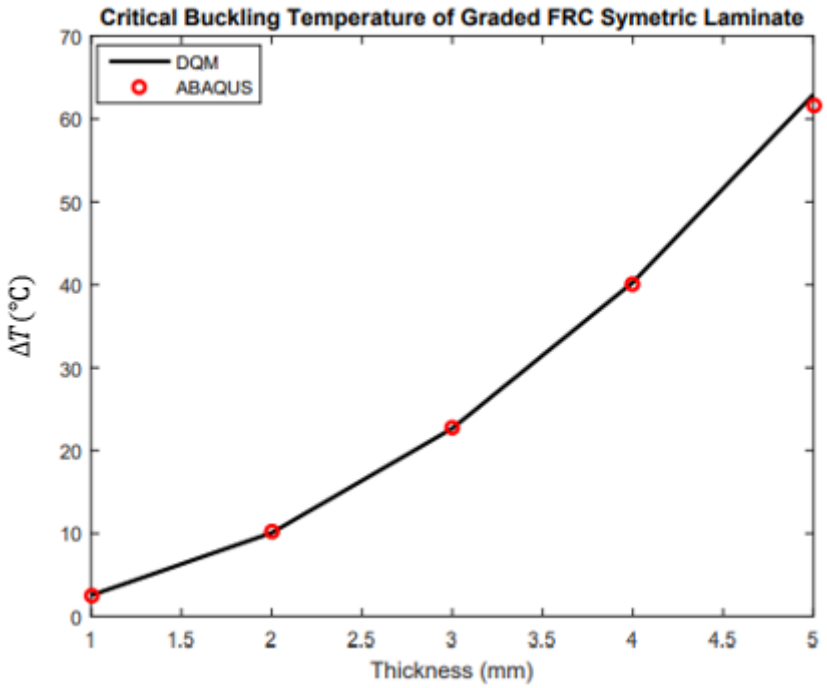

Figure 4.15. Critical buckling temperature of CCCC $[60/-30/90\ /45]_s$ angle plies composite plate with glass fiber and epoxy resin, $a = 200\ mm$,$\frac{a}{b} = 1$,$V_f(z) = 0.4(\frac{|z|}{h})$

In Figure 4.15, the critical buckling temperature was calculated for the graded fiber reinforcement composite plate with symmetrical laying angles. The change in critical buckling temperature for the composite plate clamped at all edges is seen according to the increase in thickness. The increase in thickness increases the stiffness value of the plate and the resistance of the plate against deformation becomes higher. As seen in the Figure 4.15, the critical buckling temperature increases as the thickness increases. There is also an agreement between the results of the study and the results obtained from Abaqus. When Figure 4.15 and Figure 4.8 are compared, the critical buckling temperatures of composite plates with the same configuration are different

at different boundary conditions. The critical buckling temperature value seen in clamped boundary conditions is higher than that of simply supported. This can be explained by the fact that the clamped boundary condition is a more rigid boundary.

The thickness and boundary condition of the plate whose critical buckling temperature value was calculated in Figure 4.10 was changed. The thickness value of the plate was made to 3 mm, and the critical buckling temperature value was calculated for the clamped boundary condition. The results are as in Figure 4.16.

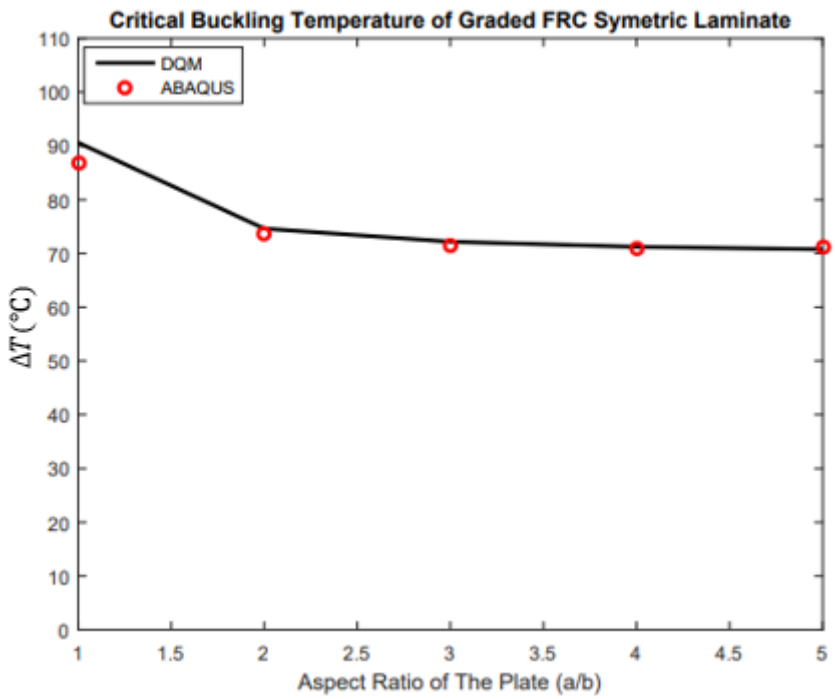

Figure 4.16. Critical buckling temperature of CCCC $[60/-30/90/45]_s$ angle plies composite plate with glass fiber and epoxy resin, $b = 100\ mm$,$h = 3.0\ mm$

$$V_f(z) = 0.4(\frac{|z|}{h})$$

In Figure 4.16, the change of critical buckling temperature according to aspect ratio is seen. As expected, when the dimensions of the plate increase, the critical buckling temperature decreases.

The boundary condition of the plate, whose critical buckling temperature was calculated for three different lamination schemes shown in Figure 4.12, was changed

to clamp. The critical buckling temperature was calculated for three different lamination schemes in the clamped boundary condition. The results obtained from DQM are shown in Figure 4.17.

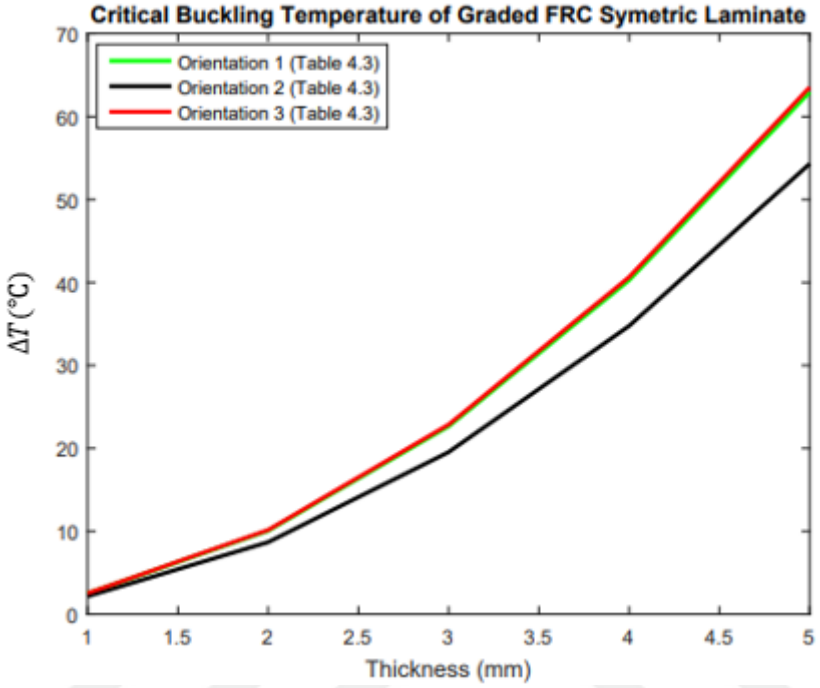

Figure 4.17. Critical buckling temperature of CCCC angle plies composite plate with glass fiber and epoxy resin from DQM, $a = 200\,mm$, $\frac{a}{b} = 1.0$, $V_f(z) = 0.4(\frac{|z|}{h})$

Critical buckling temperature of the composite plate with symmetric ply sequence was found for three fiber angle configurations at different thicknesses. The temperature values can differ with respect to orientation. It is understood from the results obtained that the fiber orientation angle affects the mechanical properties of the structure. The reason is same as in mentioned for Figure 4.12. In addition, plates with different fiber orientation angles may behave very similarly. The results in Figure 4.17 show that the critical buckling temperature values of the plate with two different fiber orientation angles can be very close.

The boundary condition of the plate, whose first four dominant buckling mode shapes are shown in Figure 4.13 and Figure 4.14, has been changed to clamp. The

first four dominant mode shapes were obtained using DQM and ABAQUS for the clamped boundary condition. The result in Figure 4.18 was obtained from DQM, and the result in Figure 4.19 was obtained from ABAQUS. When the buckling mode shapes obtained from DQM and ABAQUS are compared, it is understood that both methods give the same results.

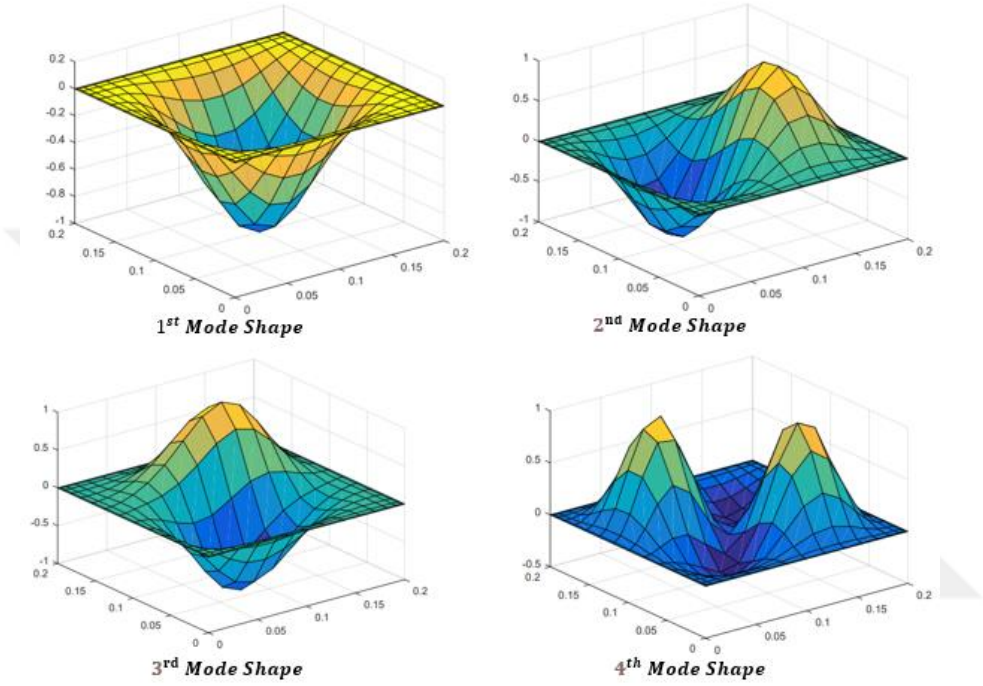

Figure 4.18. Dominant mode shapes of CCCC $[60/-30/90/45]_s$ angle plies composite plate with glass fiber and epoxy resin from DQM, $a = 200\,mm$, $\frac{a}{b} = 1.0$, $h = 1\,mm$, $V_f(z) = 0.4(\frac{|z|}{h})$

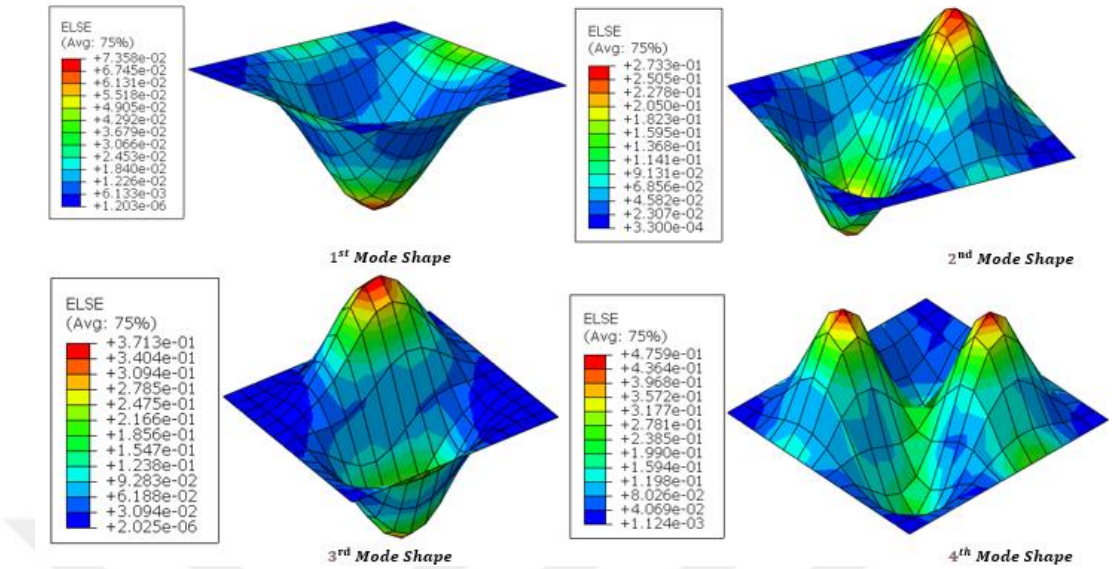

Figure 4.19. Dominant mode shapes of CCCC $[60/-30/90/45]_s$ angle plies composite plate with glass fiber and epoxy resin from ABAQUS , $a = 200\,mm$, $\frac{a}{b} = 1.0$, $h = 1\,mm$, $V_f(z) = 0.4(\frac{|z|}{h})$

4.5 Numerical Results for Unsymmetric Laminates

The plate with dimensions a, b, and h is shown in Figure 4.20. This plate has dimensions of $200x200$ mm and consists of eight plies with a laying angle of $[60/0/45/90/30/-60/45/90]$. The plate is simply- supported from all sides. The plies are composed of Glass-E-fiber and polyester resin. The composite plate is graded in the thickness direction. Gradation is provided by the fiber volume fraction changing in the z-direction. The fiber volume function is $V_f(i) = 0.4(1 - \frac{i}{N})$. Table 4.4 shows the laying angles and fiber volume fraction of the plies. The plate has an initial uniform temperature, which is then uniformly increased. After a while, it started to buckle under the axial compressive force caused by the boundary conditions at a certain temperature difference. The critical buckling temperature value that caused this load was calculated using ABAQUS and DQM for five

different plate thicknesses. The mesh density used is $13x13$, and the element type is S4R.In DQM, the plate is divided into 13 grid points, each in the x and y directions.

Plies are numbered from 1 to N when they are numbered starting from the top. i denotes one minus the examined ply number. Therefore, i takes a value from 0 to $(N-1)$. N represents total ply number.

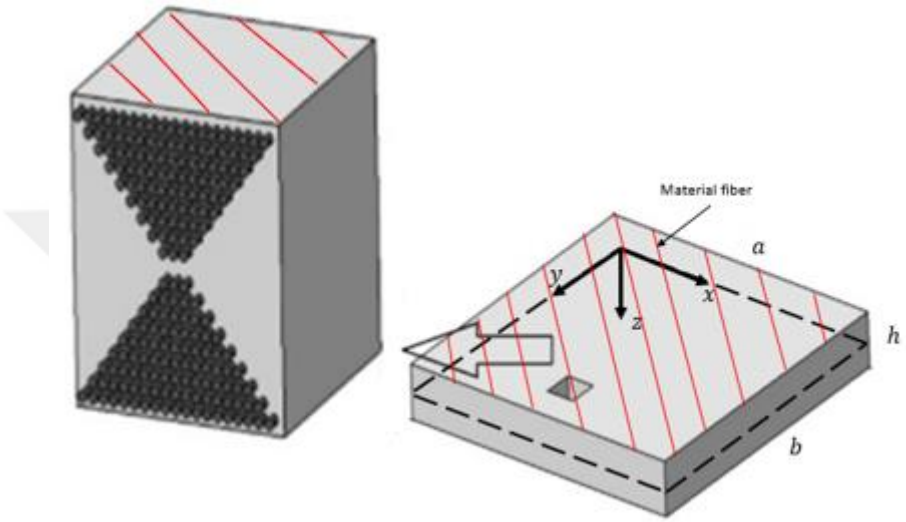

Figure 4.20. Laminated composite plate with variable fiber volume fraction

Table 4.4 Plate's lamination scheme and fiber volume fraction of each ply

Plies	V_f	**Orientation Angle (°)**
Ply 1	0.40	60
Ply 2	0.35	0
Ply 3	0.30	45
Ply 4	0.25	90
Ply 5	0.20	30
Ply 6	0.15	-60
Ply 7	0.10	45
Ply 8	0.05	90

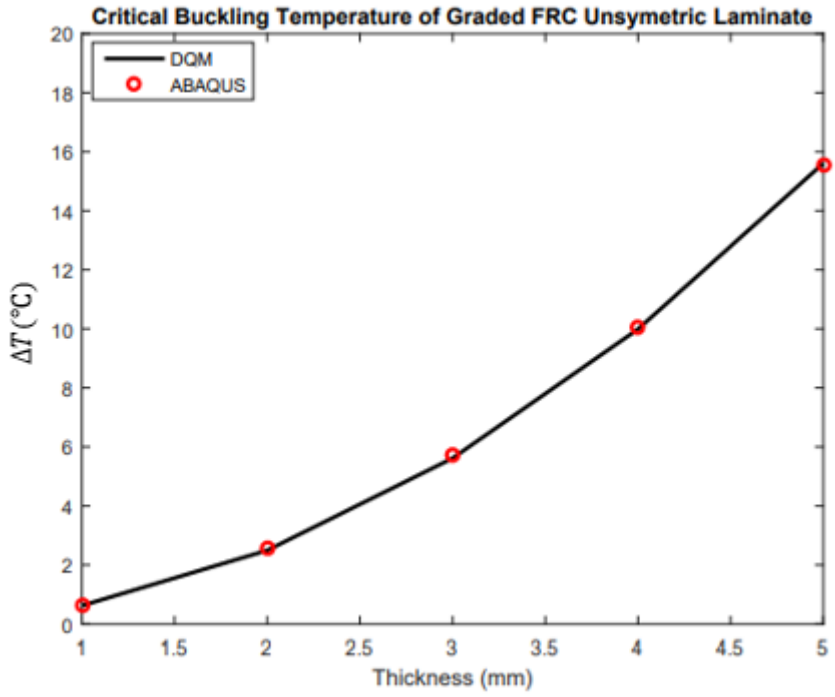

Figure 4.21. Critical buckling temperature of SSSS $[60/0/45/\ 90/30/-60/45/90]$ angle plies composite plate with glass fiber and epoxy resin, $a = 200\ mm$,$\frac{a}{b} = 1$,

$$V_f(i) = 0.4(1 - \frac{i}{N})$$

Figure 4.21 shows the critical buckling temperature values of graded fiber reinforcement composite plate with unsymmetric ply sequence. The variation of the critical buckling temperature value with the increase in thickness was investigated. The critical buckling temperature increasing according to the increase in thickness is associated with the increase in the stiffness value of the plate depending on the thickness. It is more difficult for the thicker plate to deform and switch to the bending mode. The critical buckling temperature values calculated in this study are in perfect agreement with the results in Abaqus.

Table 4.5 Critical buckling temperature of SSSS $[60/0/45/\ 90/30/-60/45/90]$ angle plies composite plate with glass fiber and epoxy resin, $a = 200\ mm$,$\frac{a}{b} = 1$, $V_f(i) = 0.4(1 - \frac{i}{N})$

Thickness (mm)	DQM (℃)	ABAQUS (℃)	Error (%)
1	0.624	0.645	3.2
2	2.497	2.562	2.6
3	5.618	5.713	1.7
4	9.987	10.050	0.6
5	15.605	15.525	0.5

The effect of some parameters on the buckling behavior of the laminated composite plate was investigated. The change in the critical buckling temperature value of the plate was investigated by changing the a/b ratio for the plate being examined. The plate is simply supported from the edges. The b value for the examined plate is 100 mm, the h value is 5 mm, and a value change. This composite plate contains eight plies consisting of Glass-E-fiber and polyester resin. The fiber volume fraction and orientation of the plies are as in Table 4.4.

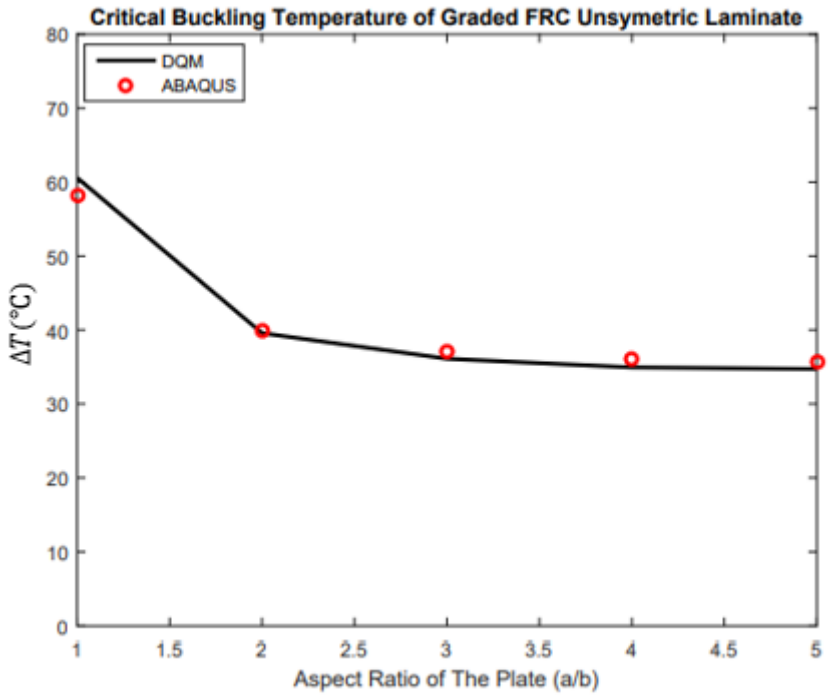

Figure 4.22. Critical buckling temperature of SSSS $[60/0/45/\ 90/30/-60/45/90]$ angle plies composite plate with glass fiber and epoxy resin, $b = 100\ mm$, $h = 5.0\ mm, V_f(i) = 0.4(1 - \frac{i}{N})$

Figure 4.22 shows the change in the critical buckling temperature value of graded fiber reinforcement composite plate with unsymmetric ply sequence according to aspect ratio. When a dimension of the plate in the direction of loading is increased, the plate's resistance to this load will decrease, so the plate's transition from in-plane compression mode to bending mode occurs at lower temperatures. Although there is a slight deviation between the calculated value and the value obtained in Abaqus, there is an agreement between the values.

Figure 4.20 shows the composite plate with dimensions a, b and h. The value of a and b is 200 mm and plate is simply- supported from all sides. The plate consists of eight plies, and there are three different combinations according to the ply laying angles. The lamination schemes of this plate are shown in Table 4.6. The material and fiber volume fraction change of the plies is the same as in the previous example. Critical buckling temperature values were calculated at five different thickness

values for three different stacking sequences. Since DQM is correlated, the critical buckling temperature value for different orientations is calculated with DQM only and the results are shown in Figure 4.23.

Table 4.6 Stacking sequences

Lamination Scheme Name	**Stacking Sequence**
Orientation 4	$[60/0/45/90/30/-60/45/90]$
Orientation 5	$[75/60/0/90/60/45/45/30]$
Orientation 6	$[90/0/45/60/75/30/60/30]$

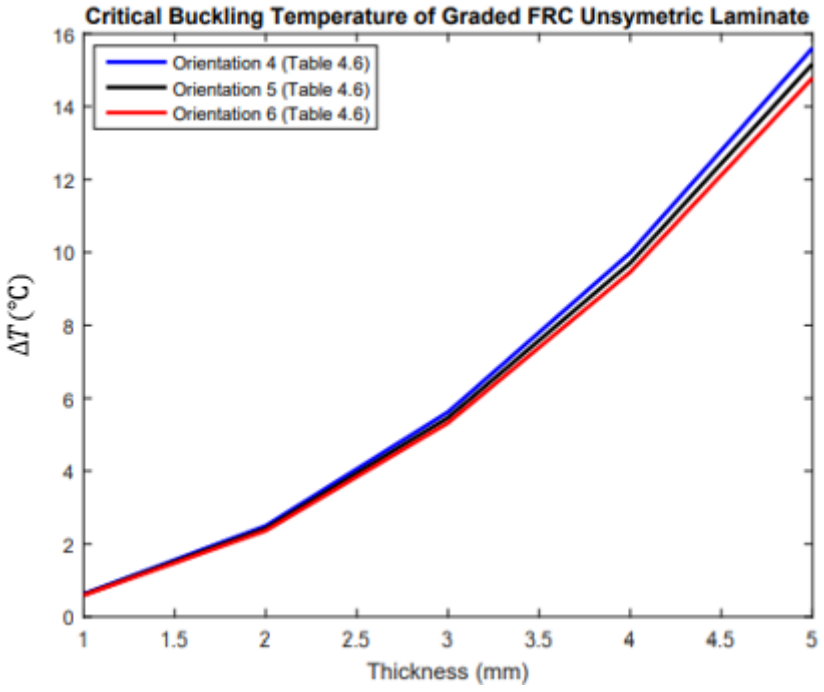

Figure 4.23. Critical buckling temperature of SSSS angle plies composite plate with glass fiber and epoxy resin, $a = 200\ mm$, $\frac{a}{b} = 1$, $V_f(i) = 0.4(1 - \frac{i}{N})$

The effect of fiber orientation angle on the buckling behavior of the structure was investigated. It has been observed that the critical buckling temperatures of the composite plate with unsymmetric ply sequence are different at different fiber

orientation angles. Most of the load in longitudinal direction is carried by the 0° angled plies ,and high percent of transverse load is carried by the 90° angled plies. Composite plates with high number of 0° and 90° angled plies carry less load; therefore, it is more difficult to buckle this plate than composite plate with less number of 0° and 90° angled plies. Laminated composite plates with the same number of 0° and 90° angled plies create more bending moment with 0° and 90° angled plies being more distant from the mid-surface. For this reason , the plate buckles easily.

The composite plate in Figure 4.20 is $200x200$ mm in size and 1 mm in thickness and is simply-supported from the edges. This composite plate consists of eight plies. Plies are composed of Glass-E-fiber and polyester resin. Ply laying angles and fiber volume fractions are shown in Table 4.4. The first four dominant mode shapes for the analysed composite plate were calculated using ABAQUS and DQM. Mode shapes obtained from DQM in Figure 4.24 and from ABAQUS in Figure 4.25 are shown. When the results from ABAQUS and DQM are examined, it is seen that the buckling mode shapes are the same.

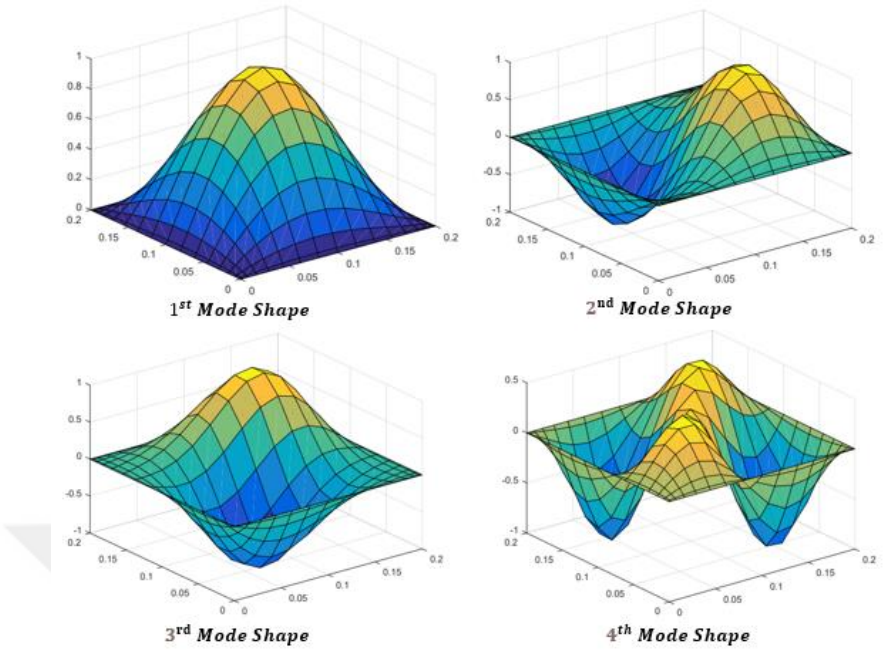

Figure 4.24. Dominant mode shapes of SSSS $[60/0/45/\ 90/30/-60/45/90]$ angle plies composite plate with glass fiber and epoxy resin from DQM,

$$a = 200\ mm\ , \frac{a}{b} = 1\ \ ,h = 1.0\ mm,\ V_f(i) = 0.4(1 - \frac{i}{N})$$

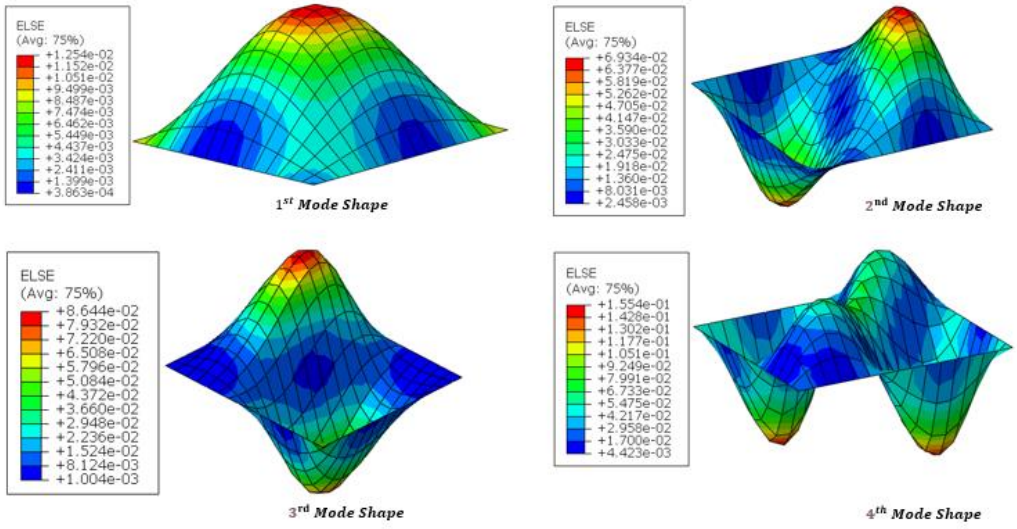

Figure 4.25. Dominant mode shapes of SSSS $[60/0/45/\ 90/30/-60/45/90]$ angle plies composite plate with glass fiber and epoxy resin from ABAQUS,

$$a = 200\ mm\ , \frac{a}{b} = 1\ \ ,h = 1.0\ mm,\ V_f(i) = 0.4(1 - \frac{i}{N})$$

The critical buckling temperature was calculated for the clamped boundary condition so that only the boundary condition was changed ,and all other parameters remained the same, as in the example in Figure 4.21.

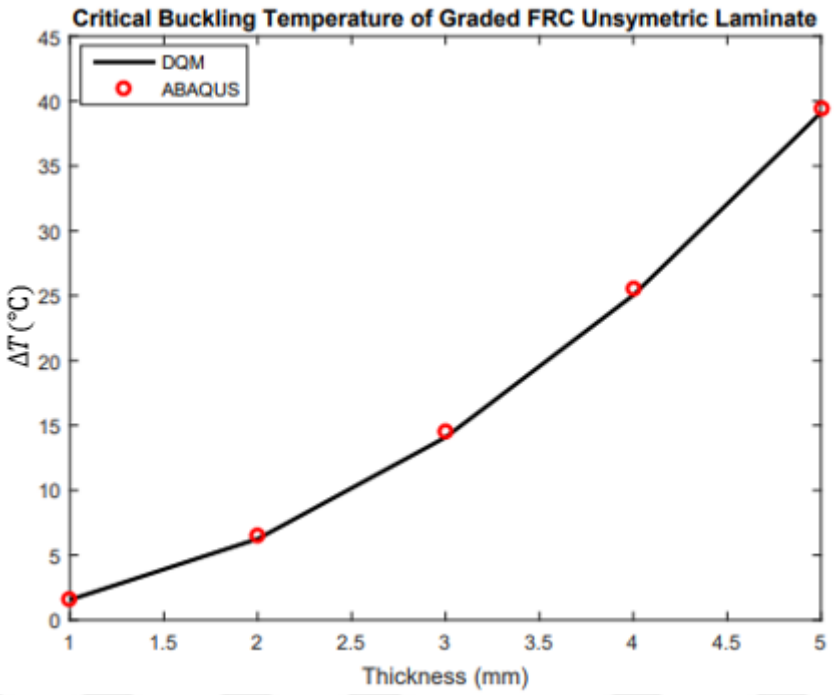

Figure 4.26. Critical buckling temperature of CCCC $[60/0/45/\ 90/30/-60/45/\ 90]$ angle plies composite plate with glass fiber and epoxy resin, $a = 200\ mm$,

$$\frac{a}{b} = 1, V_f(i) = 0.4(1 - \frac{i}{N})$$

In Figure 4.26, the critical buckling temperature value was calculated for a graded fiber reinforcement composite plate with an unsymmetric laying angle. There is a nice agreement between the results obtained in the study and the results in Abaqus. Comparing Figure 4.26 and Figure 4.21, the critical buckling temperature of the composite plate in the clamped boundary condition is higher than that of simply supported. Because clamped edge condition increases resistance to buckling mode as it reduces the half-length involved in buckling.

Table 4.7 Critical buckling temperature of CCCC $[60/0/45/\ 90/30/-60/45/90]$ angle plies composite plate with glass fiber and epoxy resin, $a = 200\ mm$, $\frac{a}{b} = 1$, $V_f(i) = 0.4(1 - \frac{i}{N})$

Thickness (mm)	DQM (℃)	ABAQUS (℃)	Error (%)
1	1.565	1.629	3.9
2	6.259	6.489	3.6
3	14.083	14.507	2.9
4	25.037	25.558	2.0
5	39.119	39.482	1.1

The change in the critical buckling temperature value according to aspect ratio is shown in Figure 4.22. The results shown in this figure were recalculated for the boundary condition clamped and thickness 3 mm. The results shown in Figure 4.27 were obtained.

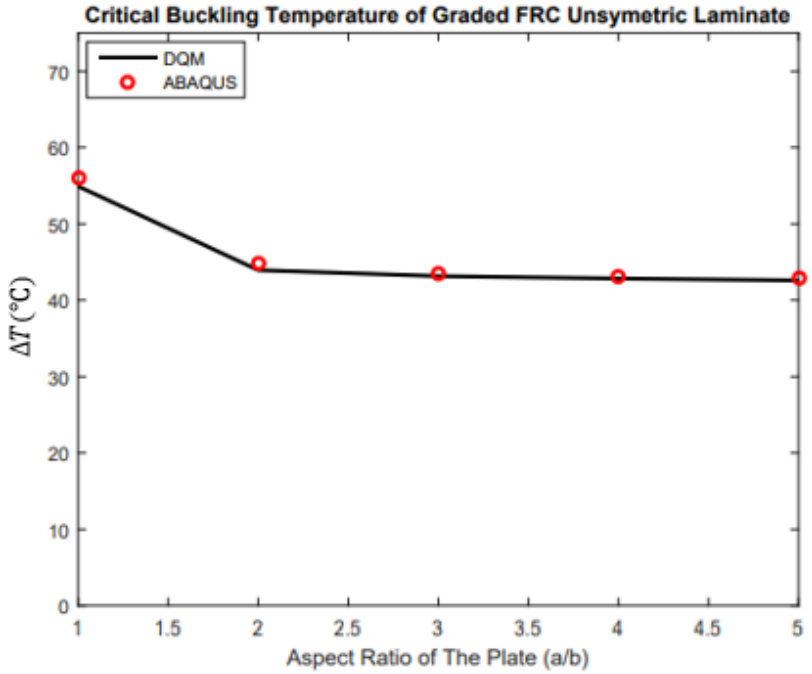

Figure 4.27. Critical buckling temperature of CCCC $[60/0/45/\ 90/30/-60/45/90]$ angle plies composite plate with glass fiber and epoxy resin, $b = 100\ mm$, $h = 3.0\ mm, V_f(i) = 0.4(1 - \frac{i}{N})$

In Figure 4.27, the change of critical buckling temperature according to aspect ratio is examined. According to the results, it was seen that the increase in plate size decreased the critical buckling temperature.

The critical buckling temperature value calculated for three different lamination schemes in Figure 4.23 was calculated by changing only the boundary condition. The values calculated for the clamped boundary condition by using DQM are given in the figure below.

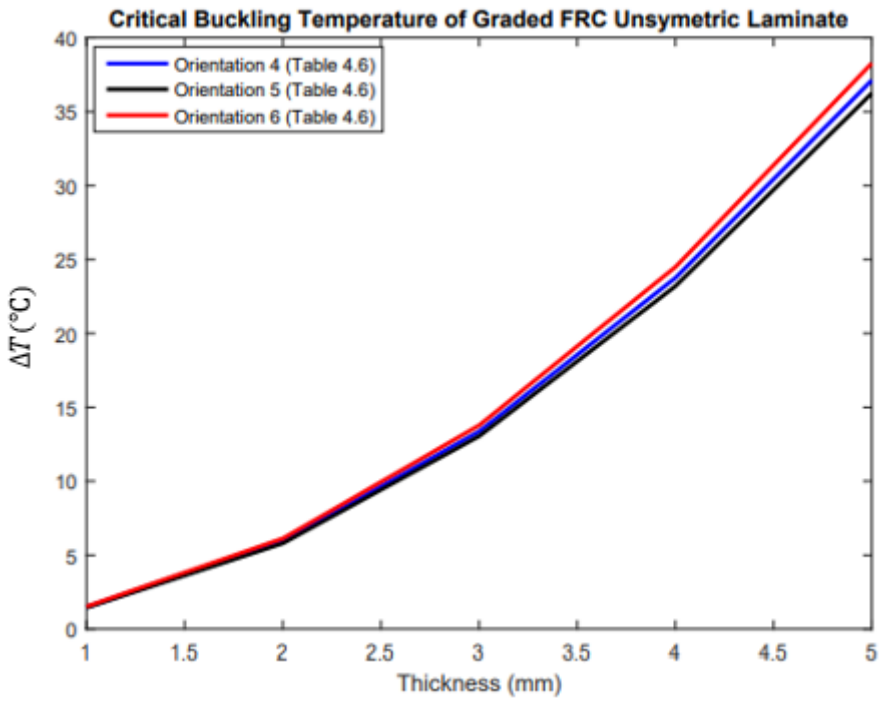

Figure 4.28. Critical buckling temperature of CCCC angle plies composite plate with glass fiber and epoxy resin, $a = 200\ mm$, $\frac{a}{b} = 1$, $V_f(i) = 0.4(1 - \frac{i}{N})$

When the results in Figure 4.28 are examined, it is seen that the fiber orientation angle affects the mechanical properties. Even though the critical buckling temperature values are very close to each other, the values differ as the lamination scheme changes. The reason is same as in mentioned for Figure 4.23.

Mode shapes calculated in simply supported boundary condition for the unsymmetric laminated composite plate were recalculated for boundary condition

clamped. All parameters except the boundary condition remained as in the example. The results are shown in Figure 4.29 and Figure 4.30. Figure 4.29 was obtained from DQM, and Figure 4.30 was obtained from ABAQUS. When the results from ABAQUS and DQM are examined, it is seen that the buckling mode shapes are the same.

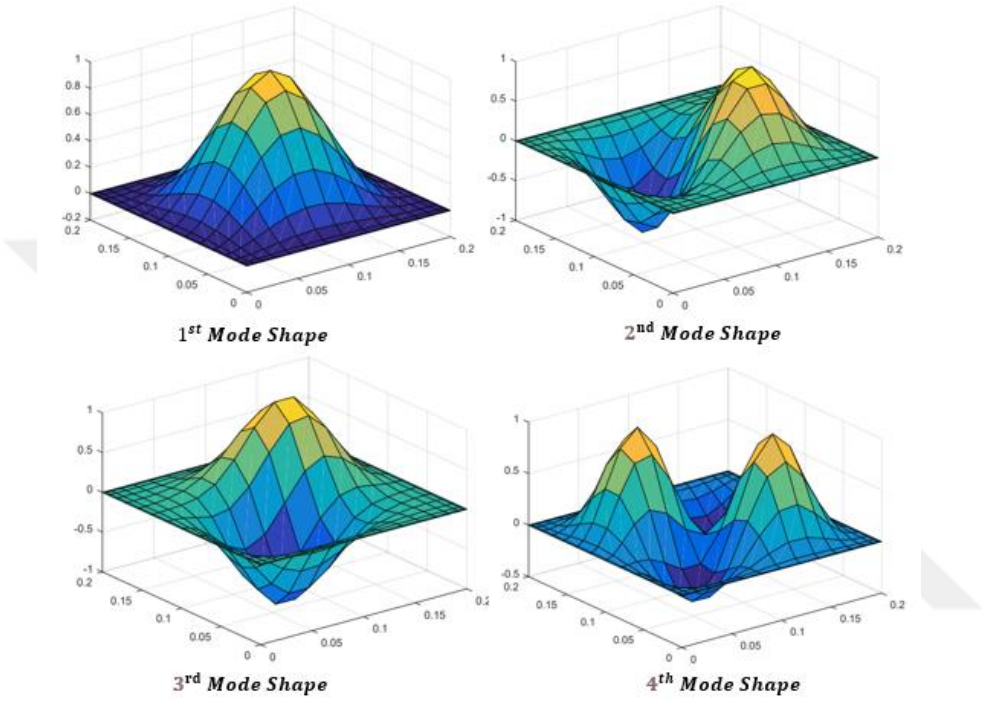

Figure 4.29. Dominant mode shapes of CCCC $[60/0/45/\ 90/30/-60/45/90]$ angle plies composite plate with glass fiber and epoxy resin from DQM,

$$a = 200\ mm\ , \frac{a}{b} = 1\ \ ,h = 1.0\ mm,\ V_f(i) = 0.4(1 - \frac{i}{N})$$

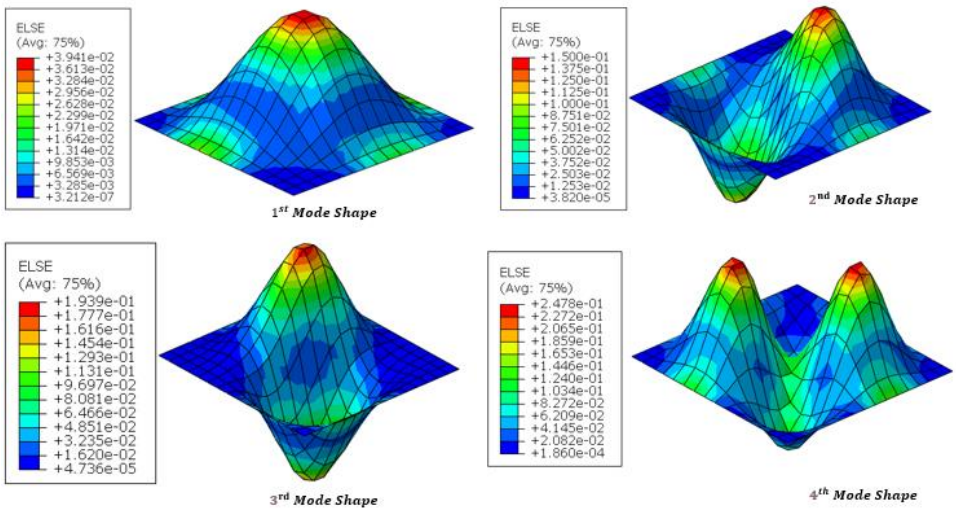

Figure 4.30. Dominant mode shapes of CCCC $[60/0/45/\ 90/30/-60/45/90]$ angle plies composite plate with glass fiber and epoxy resin from ABAQUS,

$$a = 200\ mm\ , \frac{a}{b} = 1\ \ ,h = 1.0\ mm,\ V_f(i) = 0.4(1 - \frac{i}{N})$$

CHAPTER 5

CONCLUDING REMARK AND FUTURE WORKS

This study shows the buckling behavior of graded fiber-reinforced composite plates under thermal loading. The fiber volume fraction of the investigated composite plate is different for each ply; therefore, the mechanical properties of the plate change along the thickness. Governing equations and boundary conditions were obtained with Hamilton's principle. Displacement equations were written using Kirchhoff plate theory. Since shear effects were neglected in the used theory, the behavior of thin structures was investigated. The equations obtained were solved as numeric using the differential quadrature method. When the results are compared with the studies in the literature, the accuracy of the calculations has been verified. In the numeric results shown, the critical buckling temperature, and buckling mode shapes of graded fiber-reinforced composite plates with symmetric and unsymmetric laying angles are calculated for simply supported, and all edges clamped boundary conditions. The critical buckling temperature values calculated in this thesis were compared with an article, and results were found to exactly match the paper. Since there are not enough studies on this subject, the comparison with the literature was limited. Therefore, the results obtained in the thesis were compared with the model prepared in Abaqus. For the accuracy of the prepared Abaqus model, the compared literature study was modeled with Abaqus, and the same result was found with the literature. In this way, the accuracy of the Abaqus model was tested, and comparisons were made with Abaqus. Thermal buckling analyses of graded fiber-reinforced composite plates with symmetrical laying angles were performed for simply supported and clamped boundary conditions. There is a good agreement between the critical buckling temperature value obtained in the analysis and the result obtained in Abaqus up to a certain thickness value. The shear effects arising from the increase in thickness affect the results obtained. Due to this effect, there is some deviation

between the result obtained in the study performed according to the thin plate theory and the Abaqus. When the results obtained in two different boundary conditions are examined, it is seen that the critical buckling temperature value in the clamped boundary condition is higher. These results are as expected since the clamped boundary condition is a more rigid boundary than simply supported. Thermal buckling analyses were also performed for clamped and simply supported boundary conditions for graded fiber-reinforced composite plates with unsymmetric laying angles. There is an excellent agreement between the study's results and Abaqus's results. The critical buckling temperature value in the clamped boundary condition is also higher in this plate. Finally, the buckling mode shapes of the plates were obtained. The mode shapes seen are as expected and support the study's accuracy. Unsymmetric composite plates are expected to buckle easier than symmetric composite plate because of extra moment originating from unbalance condition of unsymmetric laminated plies. In this study, it is observed that unsymmetric plate buckled at lower temperature in line with this expectation. Regardless of being symmetric and unsymmetric , the number of plies that make less angles in the direction of the load ensures that the actual structure is buckled at higher critical temperature. Therefore, the buckling behavior of plates with different lamination schemes is different since the lamination scheme affects the material properties of the structure. When plate reaches critical temperature value, buckling occurs. A sudden shape change is observed. Plate switches from in-plane compression mode to bending deformation mode. Stiffness of buckled point decreases and load carrying capacity of plate decrease. Therefore, deformation of plate becomes easy. The scope of studies for graded fiber-reinforced composite materials can be expanded. As a future work , it can be investigated how the optimum ply number and fiber volume fraction should be for the composite plate with variable fiber volume fraction, which provides the same load or temperature increase with a lower weight in order to buckle the composite plate in constant fiber volume fraction. In additive manufacturing or 3D printing, the materials used in obtaining 3D structures are added layer by layer to produce the structure. This situation is similar to laminated composite structures.

DQM can be applied to both composite structures and structures produced with additive manufacturing. For example, when calculating the material properties for homogeneous metals coming out of the nozzle layer by layer, the matrix volume fraction in the model used can be taken as zero and the material properties can be calculated layer by layer by entering E_f and V_f into the formulation. Therefore, structures produced by additive manufacturing can be analysed with the methods and models applied in this thesis. If two or more materials come out of the nozzle, analysis can be made for such materials via DQM using the material properties calculated for each layer by taking account the volume fractions and elasticity modulus of each material. A future study can be conducted on this subject. Moreover, post-buckling behavior of laminated composite plate with variable fiber volume fraction under thermal loading can be investigated for different boundary conditions as a new study.

REFERENCES

[1] Shen, H.-S., & Yang, D.-Q. (2015). Nonlinear vibration of functionally graded fiber-reinforced composite laminated cylindrical shells in hygrothermal environments. *Applied Mathematical Modelling*, *39*(5-6), 1480-1499.

[2] Shen, H.-S. (2015). Nonlinear analysis of functionally graded fiber reinforced composite laminated beams in hygrothermal environments, Part I: Theory and solutions. *Composite Structures*, *125*, 698-705.

[3] Shen, H.-S., & Zhang, C.-L. (2012). Non-linear analysis of functionally graded fiber reinforced composite laminated plates, Part I: Theory and solutions. *International Journal of Non-Linear Mechanics*, *47*(9), 1045-1054.

[4] Yas, M. H., & Aragh, B. S. (2010). Free vibration analysis of continuous grading fiber reinforced plates on elastic foundation. *International Journal of Engineering Science*, *48*(12), 1881-1895.

[5] Nejati, M., Fard, K. M., Eslampanah, A., & Jafari, S. S. (2017). Free Vibration Analysis of Reinforced Composite Functionally Graded Plates with Steady State Thermal Conditions. *Latin American Journal of Solids and Structures*, *14*(5), 886-905.

[6] Yas, M. H., & Sobhani Aragh, B. (2010). Three-dimensional analysis for thermoelastic response of functionally graded fiber reinforced cylindrical panel. *Composite Structures*, *92*(10), 2391-2399.

[7] Fu, Y., Zhang, P., & Yang, F. (2010). Interlaminar stress distribution of composite laminated plates with functionally graded fiber volume fraction. *Materials & Design*, *31*(6), 2904-2915.

[8] Tang, H., Dai, H.-L., & Liao, X. (2020). Geometrically nonlinear analysis of CFRP laminates subjected uniform load in hygrothermal effect. *Composite Structures*, *251*, 112644.

[9] Kuo, S.-Y. (2014). Aerothermoelastic analysis of composite laminates with variable fiber spacing. *Computational Materials Science*, *91*, 83-90.

[10] Leissa, A. W. (1987). A Review of Laminated Composite Plate Buckling. *Applied Mechanics Reviews*, *40*(5), 575-591.

[11] Altunsaray, E., & Bayer, İ. (2021). Buckling Analysis of Symmetrically Laminated Rectangular Thin Plates under Biaxial Compression. *Teknik Dergi*.

[12] Raju, G., Wu, Z., Kim, B. C., & Weaver, P. M. (2012). Prebuckling and buckling analysis of variable angle tow plates with general boundary conditions. *Composite Structures*, *94*(9), 2961-2970.

[13] Fares, M. E., & Zenkour, A. M. (1999). Buckling and free vibration of non-homogeneous composite cross-ply laminated plates with various plate theories. *Composite Structures*, *44*(4), 279-287.

[14] Sreehari, V. M., & Maiti, D. K. (2015). Buckling and post buckling analysis of laminated composite plates in hygrothermal environment using an Inverse Hyperbolic Shear Deformation Theory. *Composite Structures, 129,* 250-255.

[15] Kazemi, M. (2018). Hygrothermoelastic buckling response of composite laminates by using modified shear deformation theory. *Journal of Theoretical and Applied Mechanics*, 3.

[16] Han, Z. Y., Cao, Z. L., & Fu, H. Y. (2015). Buckling analysis of laminated composite plates with variable fibre orientation angle. *Materials Research Innovations*, *19*(sup5), S5-836-S5-842.

[17] Kumar, R., Patil, H. S., & Lal, A. (2015). Hygrothermoelastic Buckling Response of Laminated Composite Plates with Random System Properties: Macromechanical and Micromechanical Model. *Journal of Aerospace Engineering*, *28*(5), 04014123.

[18] Farahani, S., Fathi, M., & Nazarimofrad, E. (2020). The effect of buckling and post-buckling behavior of laminated composite plates with rotationally restrained and Pasternak foundation on stacking sequence optimization. *Scientia Iranica*, *0*(0), 0-0.

[19] Groh, R. M. J., & Weaver, P. M. (2014). Buckling analysis of variable angle tow, variable thickness panels with transverse shear effects. *Composite Structures*, *107*, 482-493.

[20] Ounis, H., Tati, A., & Benchabane, A. (2014). Thermal buckling behavior of laminated composite plates: A finite-element study. *Frontiers of Mechanical Engineering*, *9*(1), 41-49.

[21] Kuo, S.-Y., & Shiau, L.-C. (2009). Buckling and vibration of composite laminated plates with variable fiber spacing. *Composite Structures*, *90*(2), 196-200.

[22] Duran, A. V., Fasanella, N. A., Sundararaghavan, V., & Waas, A. M. (2015). Thermal buckling of composite plates with spatial varying fiber orientations. *Composite Structures*, *124*, 228-235.

[23] Malekzadeh, P., & Shojaee, M. (2013). Buckling analysis of quadrilateral laminated plates with carbon nanotubes reinforced composite layers. *Thin-Walled Structures*, *71*, 108-118.

[24] Al-Waily, M. (2015). *Analytical and numerical thermal buckling analysis investigation of unidirectional and woven reinforcement composite plate structural*. *6*(2), 125-142.

[25] Al-Waily, M., Al-Shammari, M. A., & Jweeg, M. J. (2020). An Analytical Investigation of Thermal Buckling Behavior of Composite Plates Reinforced by Carbon Nano Particles. *Engineering Journal*, *24*(3), 11-21.

[26] Sari, M. S., Ghaffari, S. S., Ceballes, S., & Abdelkefi, A. (2018). Nonlocal Buckling Characteristics of Functionally Graded Nano-Plates Subjected to Thermal Loads and Biaxial Linearly Varying Forces. *Volume 1: Development and Characterization of Multifunctional Materials; Modeling, Simulation, and Control of Adaptive Systems; Integrated System Design and Implementation*, V001T03A022.

[27] Aghazadeh, R., Dag, S., & Cigeroglu, E. (2018). Thermal effect on bending, buckling and free vibration of functionally graded rectangular micro-plates

possessing a variable length scale parameter. *Microsystem Technologies*, *24*(8), 3549-3572.

[28] Akbari Alashti, R., & Ahmadi, S. A. (2014). Buckling Analysis of Functionally Graded Thick Cylindrical Shells with Variable Thickness Using DQM. *Arabian Journal for Science and Engineering*, *39*(11), 8121-8133.

[29] Satouri, S., Kargarnovin, M. H., Allahkarami, F., & Asanjarani, A. (2015). Application of third order shear deformation theory in buckling analysis of 2D-functionally graded cylindrical shell reinforced by axial stiffeners. *Composites Part B: Engineering*, *79*, 236-253.

[30] Hajlaoui, A., Chebbi, E., & Dammak, F. (2019). Buckling analysis of carbon nanotube reinforced FG shells using an efficient solid-shell element based on a modified FSDT. *Thin-Walled Structures*, *144*, 106254.

[31] Shen, H.-S., Xiang, Y., & Lin, F. (2017). Thermal buckling and post-buckling of functionally graded graphene-reinforced composite laminated plates resting on elastic foundations. *Thin-Walled Structures*, *118*, 229-237.

[32] Lei, Z. X., Zhang, L. W., & Liew, K. M. (2016). Buckling analysis of CNT reinforced functionally graded laminated composite plates. *Composite Structures*, *152*, 62-73.

[33] Ebrahimi, F., Nouraei, M., Dabbagh, A., & Rabczuk, T. (2019). Thermal buckling analysis of embedded graphene-oxide powder-reinforced nanocomposite plates. *Advances in nano research*, *7*(5), 293-310.

[34] Shen, H.-S. (2013). Thermal buckling and post-buckling of functionally graded fiber-reinforced composite laminated plates. *Journal of Composite Materials*, *47*(22), 2783-2795.

[35] Reddy, J. N., & Wang, C. M. (1998). Deflection relationships between classical and third-order plate theories. *Acta Mechanica*, *130*(3-4), 199-208.

[36] Bellman, R., & Casti, J. (1971). Differential quadrature and long-term integration. *Journal of Mathematical Analysis and Applications*, *34*(2), 235-238.

[37] MATLAB. (2018). *9.7.0.1190202 (R2019b)*. Natick, Massachusetts: The MathWorks Inc.

[38] Smith, M. (2009). *ABAQUS/Standard User's Manual, Version 6.9*. Dassault Systèmes Simulia Corp.

[39] Reddy, J. N., & Reddy, J. N. (2004). *Mechanics of laminated composite plates and shells: Theory and analysis* (2nd ed). CRC Press.

[40] Thai, C. H., Tran, L. V., Tran, D. T., Nguyen-Thoi, T., & Nguyen-Xuan, H. (2012). Analysis of laminated composite plates using higher-order shear deformation plate theory and node-based smoothed discrete shear gap method. *Applied Mathematical Modelling*, *36*(11), 5657-5677.

[41] Nassar, M., Matbuly, M. S., & Ragb, O. (2013). Vibration analysis of structural elements using differential quadrature method. *Journal of Advanced Research*, *4*(1), 93-102.

[42] Javaheri, R., & Eslami, M. R. (2002). Thermal Buckling of Functionally Graded Plates. *AIAA Journal*, *40*(1), 162-169.

[43] Leissa, A. W. (1986). Conditions for laminated plates to remain flat under inplane loading. *Composite Structures*, *6*(4), 261-270.